Flux Spectrum Adjustment in High Flux Isotope Reactor (HFIR)

A Thesis Presented for the
Master of Science
Degree
University of Tennessee, Knoxville

Austin Clifford Stanford
December 2020

ABSTRACT

A significant portion of nuclear related research and application is dependent on the ability to utilize and improve nuclear data libraries. This has led to a tremendous amount of effort to be put in to develop and fill in the gaps in knowledge in these libraries. This analysis works to address this by categorizing and re-analyzing historical experimental data from High Flux Isotope Reactor (HFIR) in order to accurately characterize the HFIR neutron flux profile to improve precision for new experiments. If this historical data can be utilized in characterizing the neutron flux profile in HFIR to a reliable level, then it would allow for HFIR to perform high-precision new measurements. A methodology was developed for experiment information indexing by categorizing the flux into different regions, sample materials, and axial locations to create a detailed summary of important information of the experiments, which allows for more accurate comparison between samples. This re-analysis uses current nuclear data libraries to perform neutron spectral adjustment on material samples using the STAYSL PNNL suite. This analysis focuses on three distinct regions of the HFIR core: The Flux Trap, Peripheral Target Position, and Removable Beryllium regions. For each region, the chi-squared values for the fitted flux shapes remain low, implying STAYSL was able to find a neutron spectrum that fit well for each sample across all three major regions. Overall, between samples, there are low levels of variability in neutron flux, and a noticeable trend in variability decreasing for the neutron flux as the samples gets radially and axially closer to the center of the core. This holds true for each region across the entire energy spectrum. In addition, there is a clear delineation in the flux spectrum between samples from the 85 MW and the 100 MW cores in HFIR, implying distinct irradiation environments.

TABLE OF CONTENTS

INTRODUCTION AND GENERAL INFORMATION 1

1.1 Objective of Study 1

1.2 Limitations 3

1.3 General Information 4
1.3.1 Background 4
1.3.2 Literature Review 4
1.3.3 Methodology 4
1.3.4 Results 4
1.3.5 Conclusion 4

BACKGROUND AND LITERATURE REVIEW 5

2.1 HFIR 5

2.2 Regions of the Core 7
2.2.1 Flux Trap 8
2.2.2 Peripheral Target Positions 8
2.2.3 Removable Beryllium 8

2.3 Wire Characteristics 9

2.4 STAYSL PNNL 9

2.5 Literature Review 10
2.5.1 Historical Cases 10
2.5.2 Region Samples 13

METHODOLOGY 16

3.1 NJOY 16
3.1.1 Libraries 16

3.2 NJOY Post Processor (NJPP) 16

3.3 SHIELD 17

3.4 BCF 17

3.5 SigPhi Calculator 18

3.6 STAYSL PNNL 18

3.7 ENDF Data 18

3.7.1 Energy Groups....18
3.7.2 Initial Spectra....19

RESULTS AND DISCUSSIONS....23

4.1 STAYSL PNNL Results....23

4.2 Neutron Flux....28

4.3 FT-5 Comparison....33

4.4 JP1-8....37

4.5 Conclusion....40

LIST OF REFERENCES....43

VITA....47

LIST OF TABLES

Table 1: Sample Materials and Reactions 10
Table 2: Information on Operation for Historical HFIR Experiments 11
Table 3: Axial locations for samples in the FT-5 region 13
Table 4: Axial locations for samples in the PTP region 14
Table 5: Axial locations for samples in the RB-1 region 15
Table 6: Libraries for specific reactions 16
Table 7: STAYSL PNNL results for the PTP region 23
Table 8: STAYSL PNNL results for the FT-5 region 26
Table 9: STAYSL PNNL results for the RB-1 region 27
Table 10: JP 1-8 Updated activation results 38
Table 11: JP 1-8 Original and corrected result comparison 39

LIST OF FIGURES

Figure 1: Timeline of HFIR 5
Figure 2: Neutron Flux change in the HT position from the 100 MW and 85 MW HFIR cores[3] 6
Figure 3: Experimental positions in HFIR[2] 7
Figure 4: Target region positions in HFIR[2] 8
Figure 5: STAYSL PNNL suite workflow[6] 10
Figure 6: Input deck for SHIELD 17
Figure 7: Initial guess spectrum of PTP for input into STAYSL PNNL 20
Figure 8: Initial guess spectrum of FT-3/4/5 for input into STAYSL PNNL 21
Figure 9: Comparison of the fluxes for different regions including the initial guess spectrum of RB-1 for input into STAYSL PNNL 22
Figure 10: A combined flux profile of all of the samples located in the FT-5 Region 29
Figure 11: A combined flux profile of all of the samples located in the PTP Region 30
Figure 12: A combined flux profile of all of the samples located in the RB-1 Region for BOC 31
Figure 13: A combined flux profile of all of the samples located in the RB-1 Region for EOC 32
Figure 14: Flux profile for FT-5 samples > 23 cm from centerline 33
Figure 15: Flux profile for FT-5 samples between 16.5 & 22 cm from centerline 34
Figure 16: Flux profile for FT-5 samples between 10 & 16.5 cm from centerline 35
Figure 17: Flux profile for FT-5 samples between 3 & 10 cm from centerline 36
Figure 18: Flux profile for FT-5 samples < 3 cm from centerline 37
Figure 19: Flux profile for original (blue) and corrected (red) JP 1-8 experiments. Dotted black line – Average of the neutron flux in FT-5 region 40

INTRODUCTION AND GENERAL INFORMATION

Over the last few decades, numerous amounts of nuclear experiments have been performed on test reactors cross a broad array of disciplines. This has allowed the nuclear field to continue to broaden and develop with the increased amount of research opportunities. Regardless of discipline, all of these experiments hold a common trait of dependency on reliable nuclear data libraries in order to perform complex analysis. There are multiple ways to improve this data including being able to catalogue and categorize all of the available data across varying disciplines. Along with improving on current knowledge it would also help create a diverse and reliable testing ground for future data evaluations.

One such tool to accomplish this is the High Flux Isotope Reactor (HFIR) at Oak Ridge National Lab (ORNL). It has been active since the 1960's as a test reactor and isotope producer. It has been an important tool in studying material degradation and interaction in extreme conditions. Thousands of tests have been performed and documented in HFIR over its lifetime. If this historical data can be utilized in characterizing the neutron flux profile in HFIR to a reliable level, then it would allow for HFIR to perform high-precision new measurements. This analysis was written for the purpose of categorizing the historic HFIR neutron spectrum.

Reliable nuclear data is one of the fundamental tools for all nuclear related research and applications. For this reason, there has been tremendous effort to develop and fill in the gaps of knowledge in these libraries over the last few decades to improve these libraries to where they are now, only being slowed down by the time consuming process of validation and verification required for all nuclear data. This evaluated nuclear data will be critical for the future advancement of the nuclear field. There are multiple ways to improve upon nuclear data, but one more recognized belief is that major advances in nuclear data can be driven by systematic studies of compiled results from different experiments, because they offer a rich additional source of data for validation studies of present evaluations.[1] This idea can also be applied by using modern nuclear data libraries on historical studies and re-analyzing it to gain a better understanding and correct for previous uncertainties. These historical analyses helped build the understanding of how current processes work, and how materials interact with radiation. Re-analyzing these samples will allow for the re-evaluation of our understanding of these processes and improvement upon current knowledge.

1.1 Objective of Study

The focus of this analysis is to categorize and use historical experimental data to accurately categorize the HFIR neutron flux profile in order to improve precision for new experiments. HFIR was chosen as the focus of this analysis based on the wealth of current available knowledge and reliability of this data. In particular, this analysis focuses on experiments that took place in the Flux Trap (FT) region of HFIR, located at

the center of its core. In addition to the FT region, this analysis will also cover the Peripheral Target Position (PTP) region and to a lesser extent the Removable Beryllium (RB) region. These historical experiments range from the early 1980's all the way up to year 2000. L. R. Greenwood was responsible for most of the unfolding experiments, which were part of dosimetry experiments performed as part of the DOE's fusion materials research program. These experiments used sample wires of various materials placed at varying locations, both axially and radially, in the core and then performing gamma and burn-up corrections on the data to obtain activation data. The wires were selected to obtain specific reactions over a large range of incoming neutron energies. This data was then used as input into a computer code (STAYSL PNNL) to retrieve neutron flux data of the samples in the core. The varying locations of the samples are then used to create a flux map of the core.

There are several reasons for using these specific experiments: All of the experiments were performed using the same methodology of data collection, with every experiment using some combination of the five different sample wire materials of similar size and thickness. The experiments used similar methods of gamma and burn-up corrections, helping to minimizing uncertainty. The experiments take place over several decades reducing the possibility of separate experiments in HFIR interfering with the samples. Finally, the experiments take place in several different radial locations in the FT, PTP, and the Removable Beryllium regions of the core, and range +\- 25 cm vertically from the centerline, thus providing a diverse collection of data. Overall, this helps establish a basis for the data to be considered comparable and allow for appropriate correlations to be made.

This analysis will be using the nuclear activation data provided in these experiment reports to perform a re-analysis, using a modern nuclear data library, compiled for specifically for this analysis, to model the neutron flux more accurately in HFIR. This will be used to study how the neutron flux spectrum varies spatially and investigate for any biases in prior flux shape estimates arising from older nuclear data evaluations. This analysis will also work on creating a methodology for experiment information indexing by categorizing the flux into different regions, sample wire materials (reactions), and axial locations to help create a detailed summary of important information of the experiments that take place in HFIR, allowing for more accurate comparison over time. This could be used in identifying anomalies in computational models of the HFIR core and correlating the anomalies to other concurrent experiments to reduce uncertainties in errors and document outlier data. Eventually, this could establish a reliable method for analyzing how the samples interact with other material in the core.

The intention is that this analysis will help comprehensively document the wealth of historical measurement data of HFIR experiments by creating an accurate and traceable summary of experimental information. This will allow for better understanding of the neutron flux in HFIR and help identify gaps in uncertainty where current knowledge needs to improve. With proper understanding, the HFIR spectra could be used for production-quality measurements of fundamental nuclear data in the future.

1.2 Limitations

In a historical analysis that includes categorizing and re-evaluating data from almost 40 years ago there are several limitations within this analysis that could affect the quality of the data. The historical studies were brief reports that used a standard layout for each experiment making data collection easier, but lacked detailed background, discussion, or analysis. The primary goal of the neutron dosimetry data collected was in service of neutron damage rate studies in materials; thus, the spectrum unfolding was an incidental product of this work. Even so, there was an adequate amount of information to perform this analysis.

The exact level of burn-up of the core is unknown for the experiments, which may have an effect of the sample; this is more relevant for the RB region. The activation data listed in the experiments has already accounted for gamma and burn-up corrections, with just the mention of percentage changes, not allowing for validation. All of the activation rates were already converted to an effective mid-plane reaction rate, so there is a possible axial bias built-in Some of the irradiations take place for periods longer than a year and required burn-up corrections of up to 30%. However, these samples were subjected to the same method of burn-up and gamma correcting which helps mitigate the impact on the results.

Frequently, the exact target position was missing for the samples, electing to just state Target Region or Removable Beryllium. However, with the large number of total samples to compare and with how the experiments were grouped, it was possible to narrow down the locations of the samples through trial and error with reasonable assurance.

There are some more complex limitations, such as the lack of information on the contents of experiments in adjacent areas to the samples, which makes evaluation of the effects of surrounding targets or materials on the sample difficult. Trying to account for limitations such as this would be unreasonable given time and resource restraints for this analysis but cataloging the work would allow for independent study of outliers for further investigation into these effects.

All of this makes fine-tuning the neutron flux spectrum difficult as no experiment in HFIR can be performed in a vacuum, and accounting for every possible interaction would make analysis nearly impossible. So, all reasonable limitations were considered in order to create a baseline between the samples to allow for reasonable comparison. The goal of this analysis is more focused on establishing a library of historical data analyzed using the latest nuclear data libraries in order to focus future experiments to improve on the knowledge gaps.

1.3 General Information

1.3.1 Background

This section focuses on the historical background on HFIR, including discussion on its timeline, the transition from the 100 MW to the 85 MW core, the different regions of interest in HFIR. It also contains information on the wire samples used in the experiments and background on STAYSL PNNL, the code used for calculating neutron flux.

1.3.2 Literature Review

This section focuses on the information taken from the historical experiments. This includes discussion and tables of dates, exposure rates (MWd), sample regions, and the sample's axial location.

1.3.3 Methodology

This section focuses on STAYSL PNNL and its associated modules that are required for it to conduct the unfolding analysis. It also includes information on the nuclear data libraries used to create the library for STAYSL PNNL. It also contains the initial guess spectra used for each region of the core.

1.3.4 Results

This section contains the analysis of the results including tables of flux results and graphs of the HFIR neutron flux spectrums for each region using the experiments data.

1.3.5 Conclusion

This section includes discussion of the results. This includes important takeaways, uncertainties, and future experiment opportunities.

BACKGROUND AND LITERATURE REVIEW

2.1 HFIR

HFIR is a multipurpose isotope production and test reactor located at ORNL. HFIR is a beryllium-reflected, light water-cooled and moderated, flux-trap type reactor that uses highly enriched uranium-235 as the fuel. Operating at 85 MW, HFIR produces an average thermal neutron flux of 2.3 x 10^{15} n/cm^2-seconds. In the center of the core, there is a 12.7 cm diameter hole that is referred to as the “flux trap.” This is where most of the experimental targets used in this analysis are located. This analysis will also investigate the Removable Beryllium region located outside of the inner and outer fuel regions and has a significantly different flux spectrum.

For this analysis, since it is an historical analysis of HFIR cores, it should be noted that the HFIR was downgraded from 100 MW to 85 MW between 1986-1989.[2] Figure 1 shows a high-level timeline for the operation of HFIR. This corresponds to a roughly 15% decrease of the flux in the core. The hydraulic tube was located in the center of the flux trap region in the 100 MW core and was moved further away in the 85 MW core. The neutron absorption rate in the flux trap has also been lowered by the current practice of substituting aluminum dummy pins for some of the heavy-element targets, due to its relative transparency to neutrons. The total effect of the change can be seen in Figure 2, compiled from data from Mahmood’s experiment.[3] The total flux has seen almost a 30% reduction, while the shape of the curve has been smoothed reducing the difference in flux from the top/bottom to the center. The fast, intermediate, and epi-thermal fluxes are reduced by up to 25% and see similar smoothing. The thermal flux is actually increased by up to 10% or so in the 85 MW core. There are samples from before and after the core change in this analysis and the difference has been distinguished.

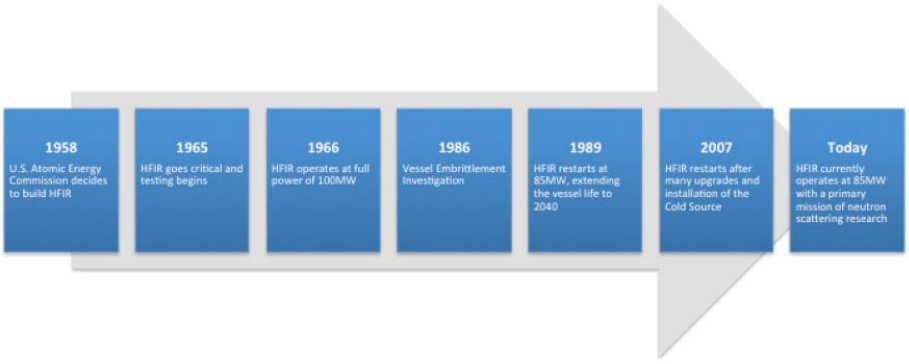


Figure 1: Timeline of HFIR

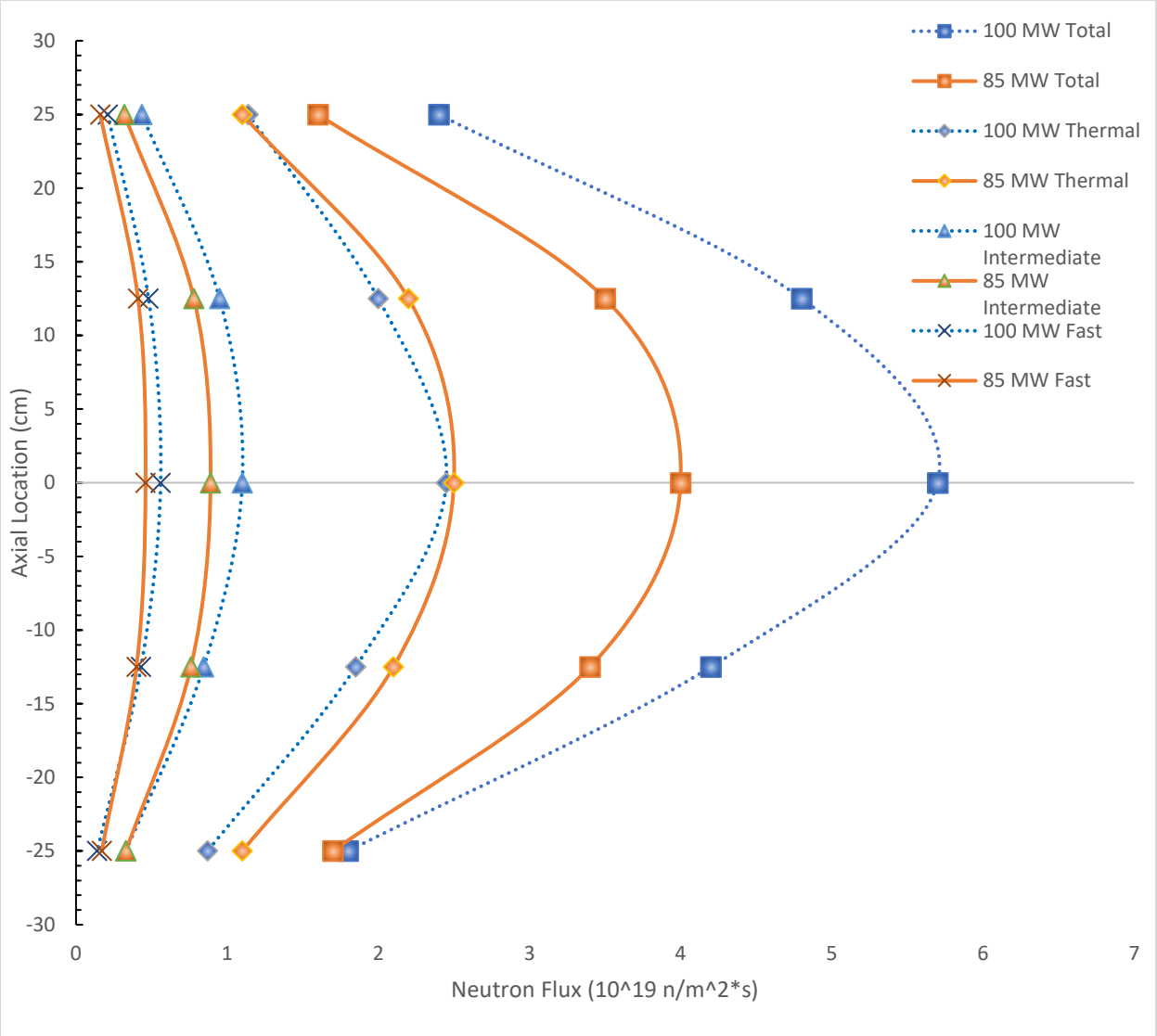


Figure 2: Neutron Flux change in the HT position from the 100 MW and 85 MW HFIR cores[3]

2.2 Regions of the Core

A flux trap occurs when there is an unfueled moderating region surrounded by fuel elements. This allows for the fast neutrons in the system to be moderated, thus creating a small region with a high thermal neutron flux. This essentially traps the neutrons, allowing for an ideal system for experimentation. In addition, the locations on the outside of the flux trap will contain a high number of fast neutrons due to the close proximity to the fuel. The flux trap in HFIR is mostly comprised of aluminum target tubes that hold the material samples.

The irradiation positions used in most experiments, including this one, are categorized into three separate regions: the flux trap region, the peripheral target position, and the Removable Beryllium (RB) reflector region. Figure 3 shows in detail the current layout of HFIR, with the Removable Beryllium surrounding the fuel region and the target region inside the ring of fuel.

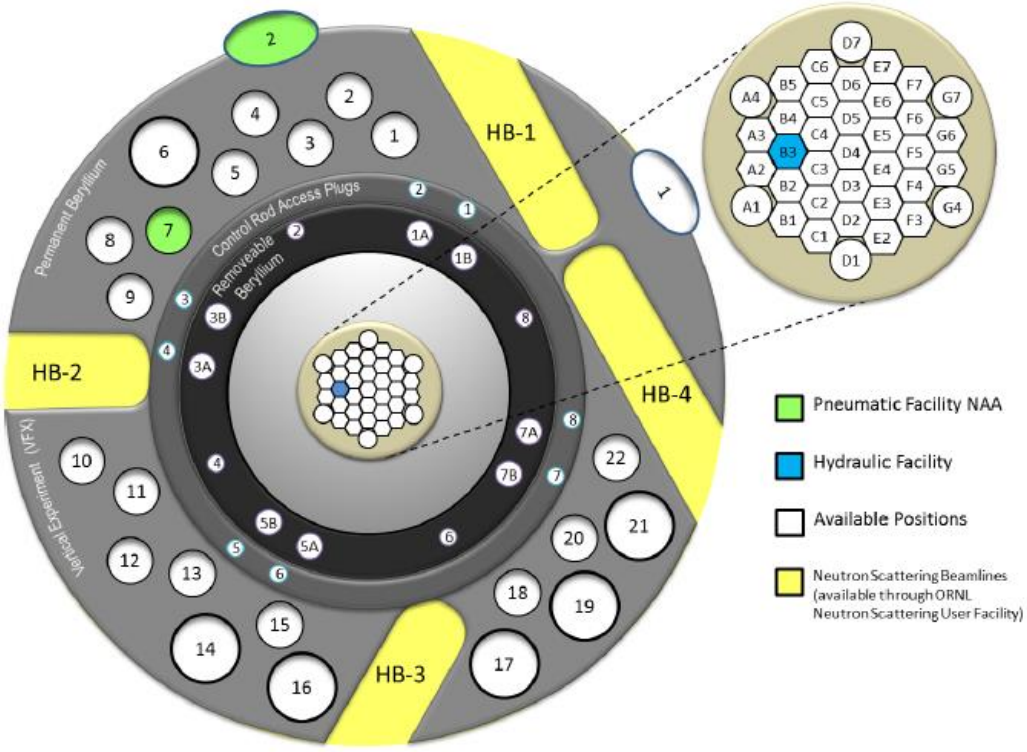


Figure 3: Experimental positions in HFIR[2]

2.2.1 Flux Trap

This region, along with PTP, is also generally referred to as the Target region in the historical experiments. This region has the highest density of thermal neutron interactions in the core and is where the majority of the experiments take place in HFIR.

2.2.2 Peripheral Target Positions

This region is located on the outside of the flux trap, close to the fuel region. Therefore, it has the highest fast neutron fluxes available to experiments in the reactor. There is a steep radial gradient change in the thermal-neutron flux at this location due to moderation.[4,5] There are only six PTP locations in HFIR, and they can be seen in Figure 4. The PTP is typically used for long term irradiations.

2.2.3 Removable Beryllium

The Beryllium Reflector region consists of concentric rings located outside of the fuel and flux trap regions. The centerline of this region is approximately 25 cm from the centerline of the reactor. There are multiple rings in the reflector, (Removable, Semi-permanent, and Permanent), but the only one of interest in this analysis is the Removable Beryllium. This is the section of the Removable Beryllium region closest to the fuel and is the most sensitive to cycle-based effects. This region can be seen in Figure 3.

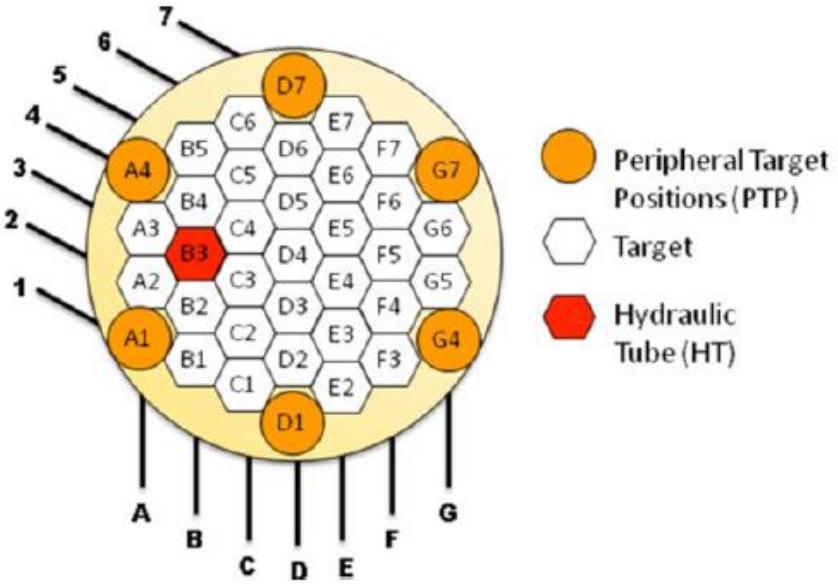


Figure 4: Target region positions in HFIR[2]

2.3 Wire Characteristics

For activation experiments in HFIR, a dosimeter is placed in a tube of varying material and loaded inside the core. A dosimeter is a sample device in the form of a wire or thin foil of a specific material. The material interacts with the neutrons in the system and initiates a nuclear reaction. The products from the reactions can then be assayed by gamma spectroscopy or another method to measure activities, in order to estimate an initial neutron spectrum. This method takes advantage of the different threshold energies for certain reactions and makes it possible to pick apart regions of the spectra by combining multiple wire measurements together to determine the flux shape. Table 1 shows the wire materials and reactions used in this analysis.

The wires used in the experiments are typically 0.020” (20 mils) in diameter. A lot of experiments use foils instead of wires, however all the cases used in this analysis use wire samples exclusively. There is reason to believe that the reaction rates have already been corrected for this and his should not have any effect on the data but should be noted.

2.4 STAYSL PNNL

STAYSL PNNL is a code that works with neutron activation rates that are measured in a reactor, accelerator, or any other neutron field to determine the neutron flux spectrum. It uses a least-squared approach to minimize the error compared to other methods such as iteration.[6] It utilizes reaction rates based on the measured activity, an initial estimate of the neutron flux spectrum, neutron activation cross sections and their associated uncertainties (covariances), and relevant correction factors. Instead of the iterative method, also referred to as unfolding, this is a neutron spectral adjustment that uses estimations provided by physics calculations to solve for an answer.

STAYSL PNNL is comprised of five separate codes that, when used in conjunction, help create an input file and library for STAYSL PNNL. Figure 5 is a simple flowchart of how STAYSL PNNL operates.

Table 1: Sample Materials and Reactions

Sample Type	Reaction(s)
Fe Wire	FE54(N,P)MN54 FE58(N,G)FE59
Ti Wire	TI46(N,P)SC46
Nb Wire	NB93(N,G)NB94
0.1% Co-Al Wire	CO59(N,G)CO60
80.2% Mn-Cu Wire	MN55(N,2N)MN54 CU63(N,A)CO60

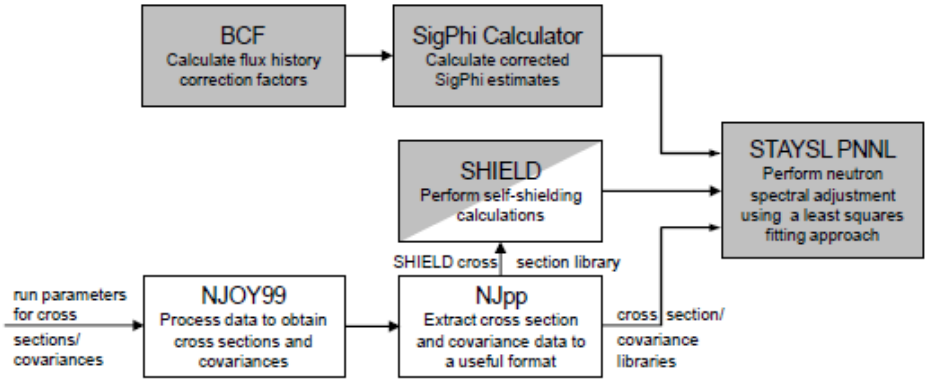


Figure 5: STAYSL PNNL suite workflow[6]

2.5 Literature Review

2.5.1 Historical Cases

The experiments used in this analysis span more than 15 years and encompass over 40 separate experiments. Each experiment is comprised of at least a few samples, including several with over a hundred individual wire samples. This makes this analysis one of the most extensive and diverse lists of historical dosimetry data from HFIR available. The irradiation time and exposure vary greatly between the samples with exposures ranging from 2,000 MWd to over 60,000 MWd. Table 2 shows a complete list of the relevant experiment information.

Table 2: Information on Operation for Historical HFIR Experiments

Report Number	Experiment	Dates	Operation Time (Days)	Exposure (MWd)
[7]DOE/ER-0045/11	T2	2/81-5/81	89 (62-119)	6,616
	RB1	11/81-7/82	242 (213-272)	23,386
[8]DOE/ER-0045/13	CTR 39	6/82-10/82	122 (93-152)	13,004
	T1	2/81-8/82	546 (519-576)	32,272
[9]DOE/ER-0045/16	JP1	1/4/84-2/1/84	28	33,634
	JP3	**5/1/84-5/28/85	392	34,009
[10]DOE/ER-0046-13	CTR 31	10/3/80-5/25/81	234	21,853
	CTR 32	8/17/80-12/12/80	117	10,863
	CTR 34, 35	12/24/81-4/17/82	114	10,614
[11]DOE/ER-0046/19	CTR 40	7/18/82-12/12/82	147	13,172
	CTR 41	8/10/82-1/5/83	148	13,208
	CTR 42-43	10/25/82-6/18/83	236	21,604
	CTR 44-45	1/30/82-5/27/83	482	10,655
[12]DOE/ER-0046/21	CTR 30	7/80-11/81	488 (458-517)	43,316
	CTR 36	11/82-4/84	517 (488-546)	38,069
	CTR 46	2/83-6/83	120 (93-149)	10,620
[13]DOE/ER-0313/2 Part 1	CTR 47-48	5/28/83-2/24/85	638	46,113
[14]DOE/ER-0313/2 Part 2	JP2	1/04/84 - 12/17/85	713	57,507
	JP6	9/11/84 - 11/14/85	429	34,677
	JP7	10/05/84 - 12/17/85	438	34,652
[15]DOE/ER-0313/3	JP4	5/01/84 - 4/18/86	717	57,909
	JP5	9/11/84 - 8/12/86	700	58,217
	JP8	10/05/84 - 9/07/86	702	58,214
[16]DOE/ER-0313/8	CTR 53-54	10/25/86 - 11/16/86	22	2,026
[17]DOE/ER-0313/19 Part 1	JP-10,11,13,16	7/20/90 - 9/19/91	426	20,279*
[18]DOE/ER-0313/19 Part 2	JP17	12/31/91 - 2/27/92	58	3,702*
	JP-18,19	8/28/91 - 10/19/91	52	3,575*
[19]DOE/ER-0313/21	JP23	12/16/93 - 6/3/94	169	9,367*
[20]DOE/ER-0313/23 Part 1	JP-9,12,15	7/20/90 - 4/1/94	1351	64,904*

Table 3 (Continued)

Report Number	Experiment	Dates	Operation Time (Days)	Exposure (MWd)
[21]DOE/ER-0313/23 Part 2	JP-20	12/16/93 - 6/3/94	169	9,367*
[22]DOE/ER-0313/26 Part 1	CTR 62-63	4/13/95 - 12/16/95	247	15,338*
[23]DOE/ER-0313/26 Part 2	TRIST ER 1-2, 7-8	3/8/96 - 6/28/96	112	6,441*

*85 MW
** The date was incorrectly listed in the historical report

2.5.2 Region Samples

The samples were separated into three distinct regions of HFIR: FT-5 (outer ring of the FT region), RB, and PTP. The samples are further differentiated by their axial distance from centerline. The locations range roughly +/- 25 cm from the midpoint of the core. These axial regions were divided into sub-regions that detail the axial location of each sample in groups in order to better reflect the flux gradients. Tables 3-5 show the range of the sub-regions as well as all of the samples that belong to them and their exact location.

Table 4: Axial locations for samples in the FT-5 region

FT-5								
Region 1	Region 2	Region 3	Region 4	Region 5	Region 6	Region 7	Region 8	Region 9
-29.28 to -22.78 cm	-22.78 to -16.27 cm	-16.27 to -9.76 cm	-9.76 to -3.25 cm	-3.25 to 3.25 cm	3.25 to 9.76 cm	9.76 to 16.27 cm	16.27 to 22.78 cm	22.78 to 29.28 cm
JP9: B (-25.3 cm)	CTR 62: C (-18.3 cm)	CTR 63: C (-15.2 cm)	JP12: B (-8.3 cm)	CTR 62: B (0 cm)	CTR 63: B (6.1 cm)	JP9: A (12 cm)	CTR 62: A (18.3 cm)	JP2: A (25.4 cm)
	JP1: E (-21 cm)	JP1: D (-12.1 cm)	JP13: D (-9.7 cm)	JP1: C (2.1 cm)	JP1: B (7.1 cm)	JP10: A (11.3 cm)	CTR 63: A (21.3 cm)	JP5: A (25.4 cm)
	JP2: F (-21 cm)	JP2: E (-12.1 cm)	JP16: D (-4.6 cm)	JP2: D (2.1 cm)	JP2: C (7.1 cm)	JP11: A (11.3 cm)	JP1: A (16.5 cm)	JP6: A (25.4 cm)
	JP3: E (-21 cm)	JP23: E (-16.1 cm)	JP23: C (-3.6 cm)	JP3: C (2.1 cm)	JP3: B (7.1 cm)	JP12: A (12.6 cm)	JP2: B (16.5 cm)	
	JP4: C (-19.3 cm)	JP3: D (-12.1 cm)	JP23: D (-7.7 cm)	JP4: B (2.1 cm)	JP5: C (7.1 cm)	JP15: A (13.1 cm)	JP3: A (16.5 cm)	
	JP6: F (-21 cm)	JP5: E (-12.1 cm)		JP5: D (2.1 cm)	JP6: C (7.1 cm)	JP16: B (10 cm)	JP4: A (17.1 cm)	
	JP8: C (-21 cm)	JP6: E (-12.1 cm)		JP6: D (2.1 cm)	JP10: B (4.6 cm)	JP23: A (13.1 cm)	JP5: B (16.5 cm)	
	JP10: E (-20.3 cm)	JP10: D (-16.2 cm)		JP7: B (2.1 cm)	JP11: B (4.6 cm)		JP6: B (16.5 cm)	
	JP11: E (-20.3 cm)	JP11: D (-16.2 cm)		JP8: B (2.1 cm)	JP16: C (4.6 cm)		JP7: A (16.5 cm)	
	JP13: E (-17.4 cm)	JP16: E (-12.8 cm)		JP10: C (-2.1 cm)	T1: A (7.22 cm)		JP8: A (16.5 cm)	
	JP16: F (-19.8 cm)			JP11: C (-2.1 cm)	T2: A (7.22 cm)		JP13: A (22.7 cm)	
				JP13: C (2.1 cm)			JP13: B (17.4 cm)	
				JP15: C (0 cm)			JP15: B (22 cm)	
				JP20: B (0 cm)			JP16: A (22.6 cm)	
				JP23: B (0.6 cm)			JP20: A (16.6 cm)	
							T1: B (16.95 cm)	
							T2: B (16.95 cm)	

Table 5: Axial locations for samples in the PTP region

PTP						
Region 1	Region 2	Region 3	Region 4	Region 5	Region 6	Region 7
-25 to -18.47 cm	-18.47 to -11.94 cm	-11.94 to -5.41 cm	-5.41 to 1.12 cm	1.12 to 7.65 cm	7.65 to 14.18 cm	14.18 to 20.71 cm
CTR 30: J (-20.8 cm)	CTR 30: I (-12.5 cm)	CTR 30: H (-8.3 cm)	CTR 30: F (0 cm)	CTR 30: E (4.2 cm)	CTR 30: C (12.5 cm)	CTR 30: A (20.8 cm)
CTR 30: K (-25 cm)	CTR 31: F (-12.5 cm)	CTR 32: H (-8.3 cm)	CTR 30: G (-4.2 cm)	CTR 31: C (4.2 cm)	CTR 30: D (8.3 cm)	CTR 30: B (16.7 cm)
CTR 31: G (-20.8 cm)	CTR 32: I (-12.5 cm)	CTR 34: F (-9.4 cm)	CTR 31: D (0 cm)	CTR 32: E (4.2 cm)	CTR 31: B (12.5 cm)	CTR 31: A (20.8 cm)
CTR 32: K (-20.8 cm)	CTR 32: J (-16.7 cm)	CTR 35: E (-9.4 cm)	CTR 31: E (-4.2 cm)	CTR 34: C (6.3 cm)	CTR 32: C (12.5 cm)	CTR 32: A (20.8 cm)
CTR 32: L (-21.9 cm)	CTR 34: G (-15.6 cm)	CTR 36: D (-10.7 cm)	CTR 32: F (0 cm)	CTR 35: C (6.3 cm)	CTR 32: D (8.3 cm)	CTR 32: B (16.7 cm)
CTR 34: H (-21.9 cm)	CTR 35: F (-15.6 cm)	CTR 40: E (-11.3 cm)	CTR 32: G (-4.2 cm)	CTR 39: A (2 cm)	CTR 34: B (12.5 cm)	CTR 34: A (18.8 cm)
CTR 35: G (-21.9 cm)	CTR 46: D (-12.7 cm)	CTR 41: E (-11.3 cm)	CTR 34: D (0 cm)	CTR 40: C (2 cm)	CTR 35: B (12.5 cm)	CTR 35: A (18.8 cm)
CTR 36: E (-20.7 cm)	CTR 47: D (-12.7 cm)	CTR 42-43: F (-6.9 cm)	CTR 34: E (-3.1 cm)	CTR 41: C (2 cm)	CTR 36: B (8.5 cm)	CTR 36: A (18.5 cm)
CTR 40: F (-20.2 cm)	CTR 48: C (-12.7 cm)	CTR 42-43: G (-11.3 cm)	CTR 35: D (-3.1 cm)	CTR 42-43: D (6.5 cm)	CTR 39: B (10.89 cm)	CTR 39: C (19.78 cm)
CTR 41: F (-20.2 cm)	CTR 53: G (-15.6 cm)	CTR 44-45: E (-11.3 cm)	CTR 36: C (-0.7 cm)	CTR 42-43: E (2 cm)	CTR 40: B (10.9 cm)	CTR 40: A (19.8 cm)
CTR 44-45: F (-20.2 cm)	CTR 54: G (-15.6 cm)	CTR 53: F (-9.4 cm)	CTR 40: D (-2.4 cm)	CTR 44-45: C (2 cm)	CTR 41: B (10.9 cm)	CTR 41: A (19.8 cm)
CTR 46: E (-21.9 cm)	JP17: D (-18.2 cm)	CTR 54: F (-9.4 cm)	CTR 41: D (-2.4 cm)	CTR 53: C (6.3 cm)	CTR 42-43: C (10.9 cm)	CTR 42-43: A (19.8 cm)
CTR 47: E (-21.9 cm)	JP18: C (-16.8 cm)	JP17: C (-10.5 cm)	CTR 44-45: D (-2.4 cm)	CTR 54: C (6.3 cm)	CTR 44-45: B (10.9 cm)	CTR 42-43: B (15.4 cm)
CTR 48: D (-21.9 cm)			CTR 46: C (0 cm)	JP19: A (3.1 cm)	CTR 46: B (12.17 cm)	CTR 44-45: A (19.8 cm)
CTR 53: H (-21.9 cm)			CTR 47: C (0 cm)		CTR 47: B (12.7 cm)	CTR 46: A (21.9 cm)
CTR 54: H (-21.9 cm)			CTR 48: B (0 cm)		CTR 53: B (12.5 cm)	CTR 47: A (21.9 cm)
JP17: E (-24.3 cm)			CTR 53: D (0 cm)		CTR 54: B (12.5 cm)	CTR 48: A (21.9 cm)
			CTR 53: E (-3.1 cm)			CTR 53: A (18.8 cm)
			CTR 54: D (0 cm)			CTR 54: A (18.8 cm)
			CTR 54: E (-3.1 cm)			JP17: A (24.1 cm)
			JP17: B (-0.9 cm)			JP18: A (22.9 cm)
			JP18: B (-4.6 cm)			
			JP19: B (-4.6 cm)			

Table 6: Axial locations for samples in the RB-1 region

RB-1							
Region 1	Region 2	Region 3	Region 4	Region 5	Region 6	Region 7	Region 8
-29.28 to -22.78 cm	-22.78 to -16.27 cm	-16.27 to -9.76 cm	-9.76 to -3.25 cm	-3.25 to 3.25 cm	3.25 to 9.76 cm	9.76 to 16.27 cm	16.27 to 22.78 cm
RB1: A (-23.02 cm)	TRIST 1-2: E (-21.34 cm)	TRIST 1-2: D (-12.17 cm)	RB1: B (-5.4 cm)	RB1: C (2.02 cm)	TRIST 1-2: B (9.17 cm)	RB1: D (10.72 cm)	RB1: E (21.15 cm)
	TRIST 7-8: E (-21.34 cm)	TRIST 7-8: D (-12.17 cm)		TRIST 1-2: C (0 cm)	TRIST 7-8: B (9.17 cm)		TRIST 1-2: A (21.34 cm)
				TRIST 7-8: C (0 cm)			TRIST 7-8: A (21.34 cm)

METHODOLOGY

3.1 NJOY

NJOY is used for extracting information from the nuclear data files in the ENDF format. For this analysis, NJOY is extracting cross section data as well as covariance data for neutron reactions. This data is then used to create nuclear data libraries for STAYSL PNNL.

Typically, this program is left untouched and users opt to use the libraries provided with the code. However, for this analysis, since a library of modern ENDF data was required, a more current version of NJOY then the one supplied with STAYSL PNNL was utilized.

3.1.1 Libraries

Covariance data is difficult to find and has changed significantly since some of these historical samples were first analyzed. For this analysis, a combination of several different libraries was used to provide the most up to date nuclear data for each material and interaction. Table 6 shows which library was used for each reaction.

3.2 NJOY Post Processor (NJPP)

NJPP parses the output from NJOY and places the cross-section data or the covariance data into a compactly structured format that will be used in SHIELD as well as STAYSL PNNL.

Table 7: Libraries for specific reactions

Reaction	Library
FE54(N,P)MN54	IRDFF-v1.05
FE58(N,G)FE59	IRDFF-v1.05
TI46(N,P)SC46	IRDFF-v1.05
NB93(N,G)NB94	JEFF-3.3
CO59(N,G)CO60	IRDFF-v1.05
MN55(N,2N)MN54	ENDF/B-VIII.0
CU63(N,A)CO60	IRDFF-v1.05

3.3 SHIELD

SHIELD is used for calculating the neutron self-shielding cross section correction factors. SHIELD is only for non-threshold reactions (non-zero cross section data down to a neutron energy of $1x10^{-4}$ eV). SHIELD is dependent on the sample configuration (dimensions and geometry) and the sample material. It is important to note, self-shielding equations for cylinders and plates are only applicable to flux monitor wires and foils that are relatively small because the they do not account for neutron scattering or flux depression effects. If larger monitors are used (with a thickness comparable to mean free path lengths for neutron scattering), then MCNP is required to correctly account for neutron self-shielding effects. This is not the case for this analysis.

For this analysis, it is assumed that the flux is isotropic in regard to the wire data. Due to the nature of reactor cores, it can be assumed that the flux coming from all directions is a better representation than a beam flux and therefore this assumption is valid. Figure 6 is a sample SHIELD input deck used for this experiment.

3.4 BCF

BCF calculates the net activity in the sample after the irradiation. Typically, it is just a production vs decay scenario in a constant power environment but can be complicated for samples that have been irradiated for either a long period of time or have gone through changes in the reactor power or beam current. The user inputs the specific history of each sample and obtains a correction factor that will be directly inputted into the SigPhi work file.

FE58G	FENG	IWX	19.69	8.4757668547E+22	ATN = (7.86 x N_a x 1) / -55.845
CO59G	CONG	IWX	19.69	1.0411511038E+20	ATN = (8.86 x N_a x 0.00115) / -58.933
MN552	MN2N	IWX	19.69	6.5669373985E+22	ATN = (7.47 x N_a x 0.802) / -54.938
NB93G	NBNG	IWX	19.69	5.5549200267E+22	ATN = (8.57 x N_a x 1) / -92.906
AU197G	AUNG	IFX	1.00	5.9068290627E+19	ATN = (19.32 x N_a x 0.001) / -196.967
AG109G	AGNG	IWX	19.69	6.3248083213E+20	ATN = (10.49 x N_a x 0.0108) / -108.905

Figure 6: Input deck for SHIELD

3.5 SigPhi Calculator

SigPhi is used to calculate corrected saturated neutron activation rates from measured activities. These are the product of the spectral-averaged neutron activation cross section and the total neutron flux. SigPhi applies the corrections for irradiation history (from BCF), gamma self-absorption, and neutron burn-up. Irradiation history corrections account for the production and decay over time. Gamma self-absorption is calculated based on the photon data and sample thickness. Neutron burn-up corrections are calculated based on the irradiation event, reaction type, and the product isotope information. An average thermal neutron fluence value is also needed to correctly estimate the burn-up.

Based on the historical experiment documentation, the data was previously corrected for gamma absorption, irradiation history, and neutron burn-up. For this reason, it is assumed no corrections were needed and the activation values from the documentation were directly inputted into the STAYSL PNNL input deck.

3.6 STAYSL PNNL

STAYSL PNNL uses all the of the library files along with the saturated reaction rates, and the estimated neutron spectrum to adjust the spectrum, based on the measured data. STAYSL PNNL uses a least-squared approach because it corrects the guess without having to iterate on flux-based calculations. The iterative process cannot take into account the full covariance matrix, which means it provides little or no information about the uncertainty of the solution. The least-squared approach includes an estimate of uncertainties and covariances for the activation data, dosimetry cross sections, and input group fluxes (each with independent probability density functions). This method is also faster, because the matrix inversion will be utilizing a smaller matrix, and an answer will almost always be found. All of this results in a statement of the uncertainties in the group fluxes due to the uncertainties of the input data. Ultimately, the least-squared fit is a better solution because the uncertainty is always minimized.

For this analysis, a normal STAYSL run was performed. This means that reaction rates and a neutron flux spectrum estimate are entered as input, resulting in adjusted outputs for the neutron spectrum.

3.7 ENDF Data

3.7.1 Energy Groups

The neutron environment differs depending on the type of reactor, but usually encompasses a range of neutron energies. The type of interaction and probability will vary greatly depending on the energy of the neutron. Energy groups are used as representatives of certain ranges instead of using a continuous distribution. Energy group sizes vary greatly depending on its use, but for this analysis the mission was to use the group size that would provide a neutron flux spectrum that gives the best fit for the measured activities.

In 2015, STAYSL PNNL was updated to incorporate new IRDFF data and extend the energy range up to 60 MeV. Five additional energy grid structures were added from NJOY to the STAYSL PNNL suite ranging from 69-group all the way to 640-/725-group. For this analysis, the 725-group structure was chosen in order to give the best granularity. In addition to the 725-group input that STAYSL PNNL uses to calculate the flux spectrum, a second user-specified energy grid can be placed into the input file to dictate how the results will be displayed. STAYSL PNNL will interpolate the flux into this grid in the output.

For this analysis, a 252-group grid was specified as the output from STAYSL PNNL. The 252-group refers to the AMPX master library group structure used by SCALE. It is the standard library, because it is optimized for thermal systems and uses weighting functions specific for the Light Water Reactor (LWR) spectrum.

3.7.2 Initial Spectra

STAYSL PNNL requires an initial guess spectrum in order to perform the calculation. STAYSL PNNL is able to perform the calculation as long as the initial spectrum resembles a spectrum even if the values are significantly different. To reduce possible errors, the initial spectrum guess was built to look similar to the expected final results, based on a previous MCNP model of HFIR Cycle 400.[24]

Figures 7-9 show the initial guess spectra for the PTP, FT-5, and RB-1 regions. All of the regions follow a similar shape with the distinct difference being the increased flux at locations closer to center of the flux trap region. The FT is comprised of three sections, FT-3/4/5. FT-3 is closest to the center of the flux trap region, while FT-5 is in close proximity to the PTP region, and FT-4 in the middle of FT-3 and 5. RB-1 also includes a Beginning-of-Cycle (BOC) and End-of-Cycle (EOC) model to account for core burn-up differences during operation.

PTP Initial Guess Spectrum

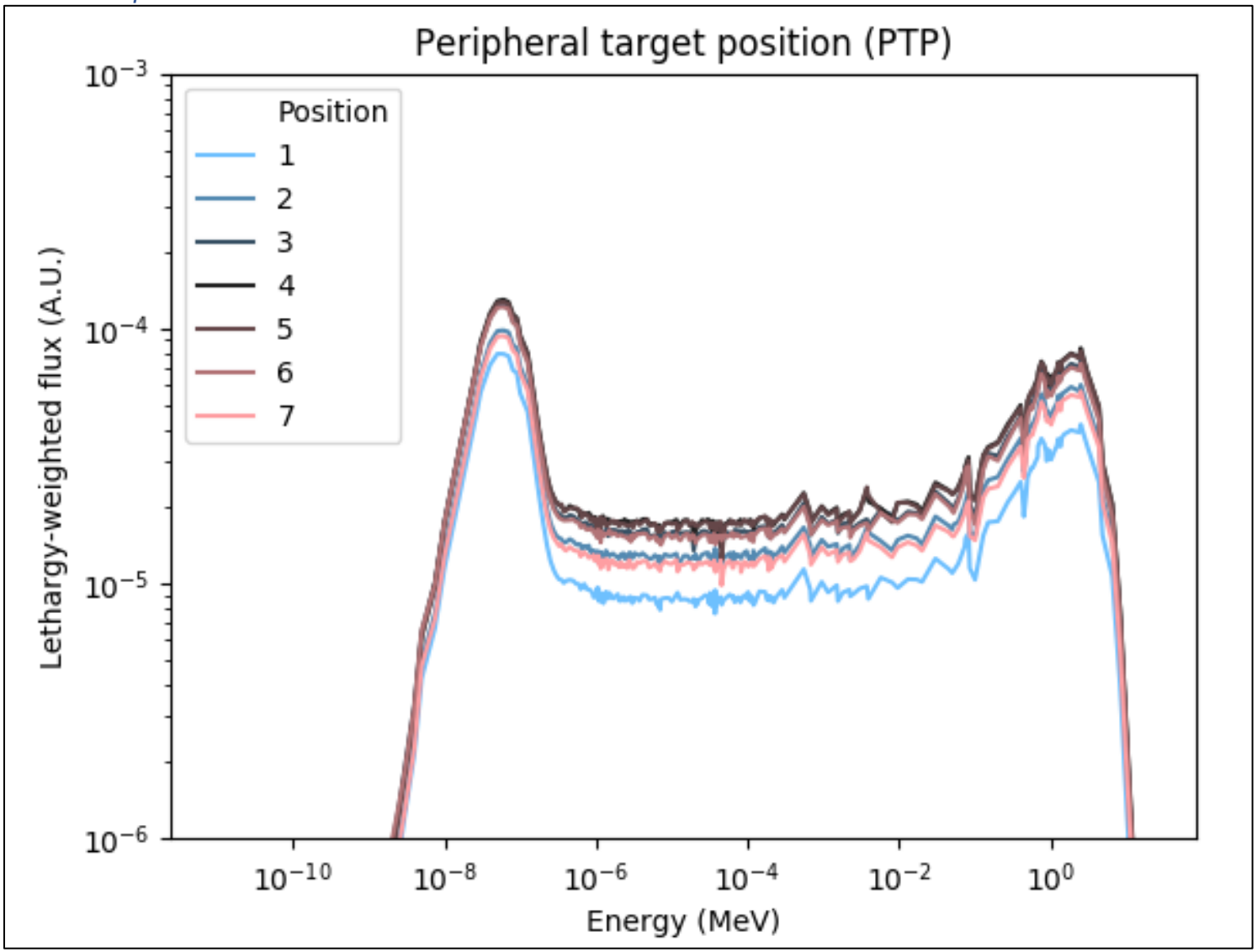


Figure 7: Initial guess spectrum of PTP for input into STAYSL PNNL

Flux Trap Initial Guess Spectrums

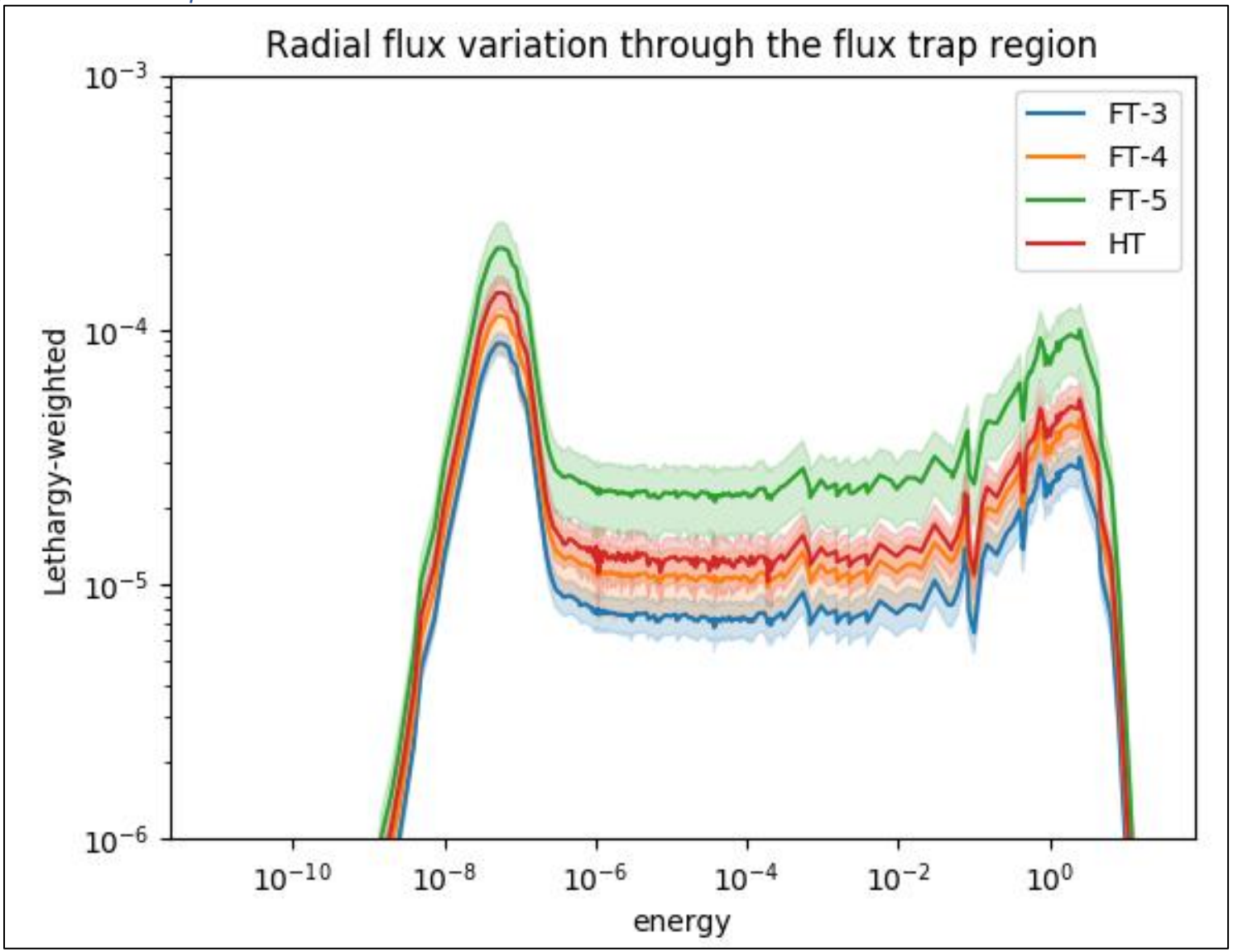


Figure 8: Initial guess spectrum of FT-3/4/5 for input into STAYSL PNNL

RB-1 Initial Guess Spectrums

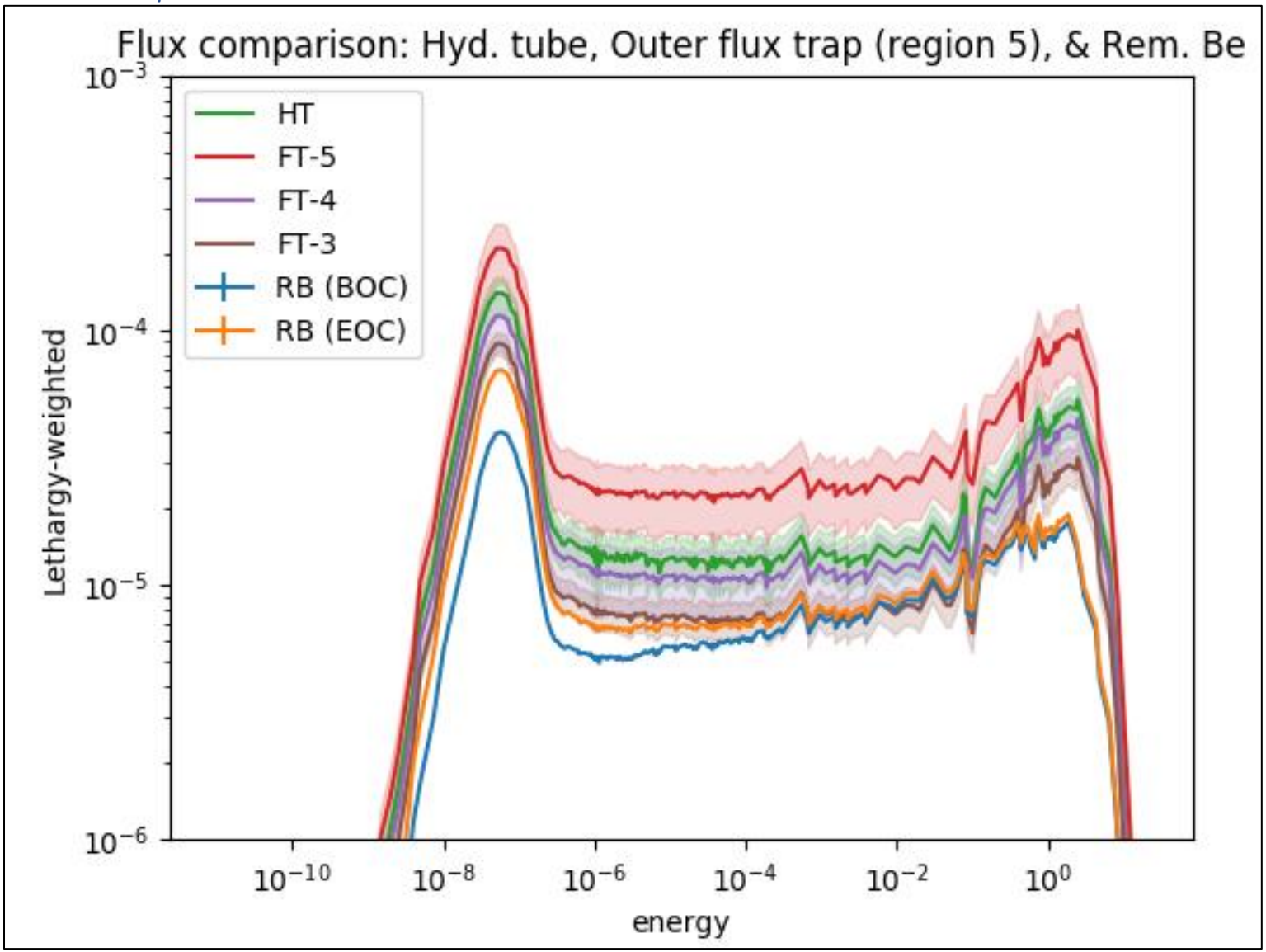


Figure 9: Comparison of the fluxes for different regions including the initial guess spectrum of RB-1 for input into STAYSL PNNL

RESULTS AND DISCUSSIONS

Using the STAYSL PNNL input decks and the library files created for this analysis, STAYSL PNNL calculated a neutron flux profile for each individual sample. In addition to the neutron flux, each sample has a chi-squared value that measures how well the distribution of data fits with the expected results.

Section 4.1 contains tables listing the important sample information along with the normalized chi-squared values.

Section 4.2 contains the neutron flux spectra for each region including a BOC and EOC for the RB-1 region.

Section 4.3 is a breakdown of the FT-5 region in order to show how the axial distance from the centerline affects the variability of the neutron flux results.

Section 4.4 goes into depth on the JP 1-8 experiment series, which required the original activation rates to be corrected and the method and justification for it.

4.1 STAYSL PNNL Results

Tables 7-9 show an overall low variability among the chi-squared values across all regions. There are a few outliers, but on average the reduced chi-squared value stays below 5. This would indicate that STAYSL was able to find a neutron spectrum that fit well for each sample across all three major regions.

A few things to note: During initial runs, the self-shielding factors were negligible for these sample monitors, under a few percent, so they were left out of the final STAYSL PNNL input decks. Second, experiments with only one type of sample wire always find an exact match and cannot calculate a chi-squared value. For this reason, they were excluded from the tables. Finally, Mn-55 sample wires consistently had a higher standard deviation than any of the other sample types.

Table 8: STAYSL PNNL results for the PTP region

Report Number	Experiment	Experiment Location	Location Used	Sample ID	Height (cm)	Region Used	Reduced Chi-Squared
DOE/ER-0045-13	CTR 39	PTP	PTP	A	2	5	1.79
				B	10.89	6	1.26
				C	19.78	7	1.00
DOE/ER-0046-19	CTR 40	PTP	PTP	A	19.8	7	0.66
				B	10.9	6	2.34
				C	2	5	0.79
				D	-2.4	4	2.08
				E	-11.3	3	1.19
				F	-20.2	1	2.65

Table 9 (Continued)

Report Number	Experiment	Experiment Location	Location Used	Sample ID	Height (cm)	Region Used	Reduced Chi-Squared
	CTR 41	PTP	PTP	A	19.8	7	0.66
				B	10.9	6	2.34
				C	2	5	0.79
				D	-2.4	4	2.08
				E	-11.3	3	1.19
				F	-20.2	1	2.65
	CTR 42-43	PTP	PTP	A	19.8	7	0.75
				B	15.4	7	0.91
				C	10.9	6	1.09
				D	6.5	5	1.15
				E	2	5	1.51
				F	-6.9	3	1.03
				G	-11.3	3	1.04
	CTR 44-45	PTP	PTP	A	19.8	7	2.15
				B	10.9	6	1.39
				C	2	5	1.89
				D	-2.4	4	1.47
				E	-11.3	3	1.32
				F	-20.2	1	1.82
DOE/ER-0046-13	CTR 31	PTP	PTP	A	20.8	7	0.22
				B	12.5	6	2.58
				C	4.2	5	16.61
				D	0	4	6.13
				E	-4.2	4	5.37
				F	-12.5	2	6.40
				G	-20.8	1	4.75
	CTR 32	PTP	PTP	A	20.8	7	3.35
				B	16.7	7	6.29
				C	12.5	6	5.37
				E	4.2	5	3.14
				G	-4.2	4	4.09
				H	-8.3	3	4.82
				I	-12.5	2	9.76
				K	-20.8	1	3.87
	CTR 34	PTP	PTP	A	18.8	7	1.09
				B	12.5	6	1.50
				C	6.3	5	2.86
				E	-3.1	4	1.91
				F	-9.4	3	2.99
				G	-15.6	2	2.09
				H	-21.9	1	1.94
	CTR 35	PTP	PTP	A	18.8	7	2.69
				B	12.5	6	2.79
				C	6.3	5	2.94
				E	-9.4	3	3.59
				F	-15.6	2	2.14
				G	-21.9	1	3.16
DOE/ER-0046-21	CTR 30	PTP	PTP	A	20.8	7	1.23
				C	12.5	6	0.42
				E	4.2	5	0.37
				G	-4.2	4	0.29
				I	-12.5	2	5.13
				J	-20.8	1	4.70
	CTR 36	PTP	PTP	A	18.5	7	1.14
				B	8.5	6	3.26
				C	-0.7	4	1.26
				D	-10.7	3	1.97
				E	-20.7	1	5.27
	CTR 46	PTP	PTP	A	21.9	7	1.16
				B	12.7	6	1.80
				C	0	4	3.44

Table 10 (Continued)

Report Number	Experiment	Experiment Location	Location Used	Sample ID	Height (cm)	Region Used	Reduced Chi-Squared
DOE/ER-0313-2 Part 1	CTR 47	PTP	PTP	A	21.9	7	0.38
				B	12.7	6	2.80
				C	0	4	0.04
				D	-12.7	2	0.52
				E	-21.9	1	2.57
	CTR 48	PTP	PTP	A	21.9	7	0.07
				B	0	4	0.48
				C	-12.7	2	0.35
				D	-21.9	1	2.35
DOE/ER-0313-8	CTR 53	PTP (A1 & A4)	PTP	A	18.8	7	2.60
				B	12.5	6	9.20
				C	6.3	5	0.84
				D	0	4	1.64
				E	-3.1	4	1.85
				F	-9.4	3	0.99
				G	-15.6	2	2.74
				H	-21.9	1	7.22
	CTR 54	PTP (A1 & A4)	PTP	A	18.8	7	2.17
				B	12.5	6	1.31
				C	6.3	5	1.36
				D	0	4	0.58
				E	-3.1	4	2.29
				F	-9.4	3	4.27
				G	-15.6	2	0.23
				H	-21.9	1	0.62
DOE/ER-0313-19 Part 2	JP17	PTP	PTP	A	24.1	7	0.37
				B	-0.9	4	1.97
				C	-10.5	3	1.19
				D	-18.2	2	3.16
				E	-24.3	1	0.43
	JP18	B-1	PTP	A	22.9	7	3.05
				B	-4.6	4	2.22
				C	-16.8	2	2.43
	JP19	E-7	PTP	A	3.1	5	3.54
				B	-4.6	4	4.43

Table 11: STAYSL PNNL results for the FT-5 region

Report Number	Experiment	Experiment Location	Location Used	Sample ID	Height (cm)	Region Used	Reduced Chi-Squared
DOE/ER-0045-11	T2	FT-5	FT-5	A	7.22	6	1.12
				B	16.95	8	0.17
DOE/ER-0045-13	T1	FT-5	FT-5	A	7.22	5	0.28
				B	16.95	7	0.98
DOE/ER-0045-16	JP1	FT-5	FT-5	A	16.5	8	0.50
				B	7.1	6	3.97
				C	2.1	5	2.72
				D	-12.1	3	1.98
				E	-21	2	0.67
	JP3	FT-5	FT-5	A	16.5	8	0.72
				B	7.1	6	1.48
				C	2.1	5	1.10
				D	-12.1	3	0.59
				E	-21	2	1.33
DOE/ER-0313-2 Part 2	JP2	FT-5	FT-5	A	25.4	9	0.06
				B	16.5	8	1.02
				C	7.1	6	1.09
				D	2.1	5	1.73
				E	-12.1	3	1.27
				F	-21	2	0.50
	JP6	FT-5	FT-5	A	25.4	9	1.13
				B	16.5	8	1.52
				C	7.1	6	6.46
				D	2.1	5	6.39
				E	-12.1	3	3.65
				F	-21	2	0.97
	JP7	FT-5	FT-5	A	16.5	8	0.92
				B	2.1	5	5.40
DOE/ER-0313-3	JP4	FT-5 (B1 & E7)	FT-5	A	17.1	8	3.41
				B	2.1	5	1.24
				C	-19.3	2	4.59
	JP5	FT-5 (B1 & E7)	FT-5	A	25.4	9	8.39
				B	16.5	8	2.52
				C	7.1	6	0.04
				D	2.1	5	0.92
				E	-12.1	3	1.24
	JP8	FT-5 (B1 & E7)	FT-5	A	16.5	8	2.88
				B	2.1	5	2.80
				C	-21	2	8.99
DOE/ER-0313-19 Part 1	JP10	FT-5 (4.47 cm)	FT-5	A	11.3	7	3.54
				B	4.6	6	3.42
				C	-2.1	5	2.05
				D	-16.2	3	1.47
				E	-20.3	2	1.26
	JP11	FT-5 (4.47 cm)	FT-5	A	11.3	7	3.48
				B	4.6	6	2.28
				C	-2.1	5	1.89
				D	-16.2	3	2.99
				E	-20.3	2	1.12
	JP13	FT-5 (4.47 cm)	FT-5	A	22.7	8	0.77
				B	17.4	8	1.52
				C	2.1	5	3.69
				D	-9.7	4	5.54
				E	-17.4	2	3.14
	JP16	FT-5 (4.47 cm)	FT-5	A	22.6	8	1.38
				B	10	7	2.65
				C	4.6	6	5.02
				D	-4.6	4	5.17
				E	-12.8	3	4.44
				F	-19.8	2	3.97

Table 12 (Continued)

Report Number	Experiment	Experiment Location	Location Used	Sample ID	Height (cm)	Region Used	Reduced Chi-Squared
DOE/ER-0313-21	JP23	FT-5 (TP G-6)	FT-5	A	13.1	7	0.43
				B	0.6	5	0.46
				C	-3.6	4	0.71
				D	-7.7	4	0.62
				E	-16.1	3	0.67
DOE/ER-0313-23 Part 1	JP9	FT-5 (4.47 cm)	FT-5	A	12	7	0.37
				B	-25.3	1	0.22
	JP12	FT-5 (4.47 cm)	FT-5	A	12.6	7	1.23
				B	-8.3	4	1.24
	JP15	FT-5 (4.47 cm)	FT-5	A	13.1	7	0.53
				B	22	8	2.27
				C	0	5	1.64
DOE/ER-0313-23 Part 2	JP20	FT-5 (4.47 cm)	FT-5	A	16.6	8	0.70
				B	0	5	0.40
DOE/ER-0313-26 Part 1	CTR 62	FT-5 (4.47 cm)	FT-5	A	18.3	8	3.71
				B	0	5	1.40
				C	-18.3	2	2.04
	CTR 63	FT-5 (4.47 cm)	FT-5	A	21.3	8	3.10
				B	6.1	6	2.20
				C	-15.2	3	0.67

Table 13: STAYSL PNNL results for the RB-1 region

Report Number	Experiment	Experiment Location	Location Used	Sample ID	Height (cm)	Region Used	Reduced Chi-Squared (BOC)	Reduced Chi-Squared (EOC)
DOE/ER-0045-11	RB1	RB	RB1	C	2.02	5	1.78	2.23
				D	10.72	7	1.62	2.95
				E	21.15	8	1.07	3.35
DOE/ER-0313-26 Part 2	TRIST 1-2	RB	RB1	A	21.34	8	0.78	2.41
				B	9.17	6	0.79	1.65
				C	0	5	0.14	1.25
				D	-12.17	3	1.01	1.00
				E	-21.34	2	0.97	0.97
	TRIST 7-8	RB	RB1	A	21.34	8	0.97	5.33
				B	9.17	6	1.01	2.80
				C	0	5	0.93	1.99
				D	-12.17	3	1.28	1.75
				E	-21.34	2	2.12	2.77

4.2 Neutron Flux

Figures 10-13 show the neutron flux profiles for each sample. The samples are graphed according to the region they are located in, with line colors corresponding to the axial distance from centerline.

Figure 10 shows the FT-5 region with the flux profile closely resembling the initial guess spectrum. The results show the clear flux magnitude differences between the different axial regions as you move away from the centerline, but with no major variance in shape between them. Overall, the FT-5 Region shows low level of variability in neutron flux.

Figure 11 shows the PTP region also has a flux profile closely resembling the initial guess spectrum. Again, the graph shows the differences in magnitude between the axial sub-regions, however you can see even lower variability between the samples, with each sub-region tightly grouped together. This is partially attributed to the smaller number of sub-regions even though the groups have an increased range. Overall, the PTP Region also shows low level of variability in neutron flux.

Figures 12-13 show the RB-1 region also has a flux profile closely resembling the initial guess spectrum. From inspection, there is virtually no difference between the BOC and EOC samples besides minor magnitude differences. This can be partially attributed to the smaller number of experiment samples. In contrast to the FT and PTP regions, there is noticeable difference in neutron flux magnitude in relation to axial distance from the centerline. The samples have separated into two distinct groups with the bottom group consisting of samples located more than 15 cm from the centerline. This trend continues along the entire energy spectrum but is more noticeable in the thermal and epi-thermal regions. Even with these differences, the RB-1 region also shows low level overall variability in neutron flux, with the condition of being more sensitive to axial differences than the FT-5 and PTP regions.

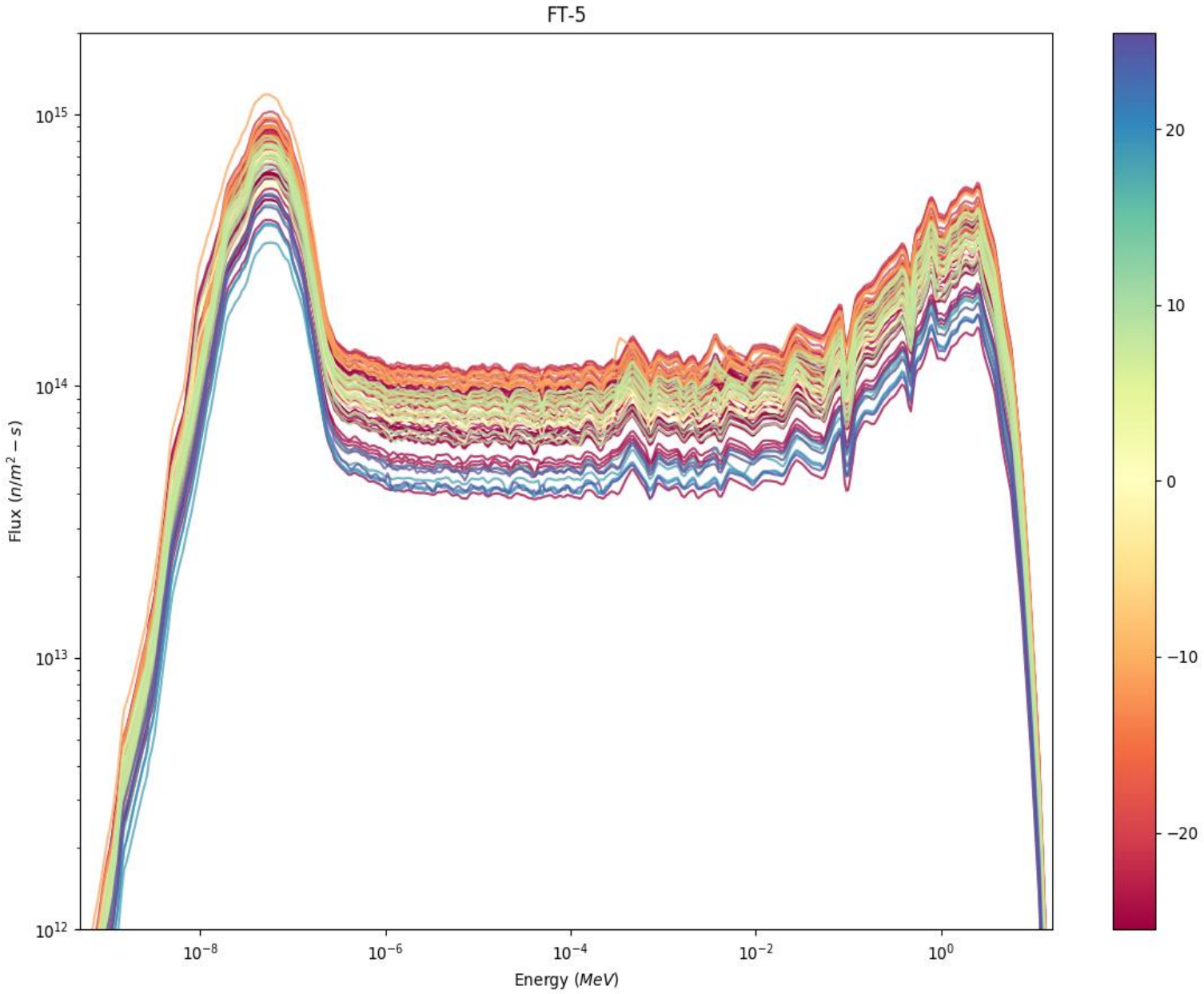


Figure 10: A combined flux profile of all of the samples located in the FT-5 Region

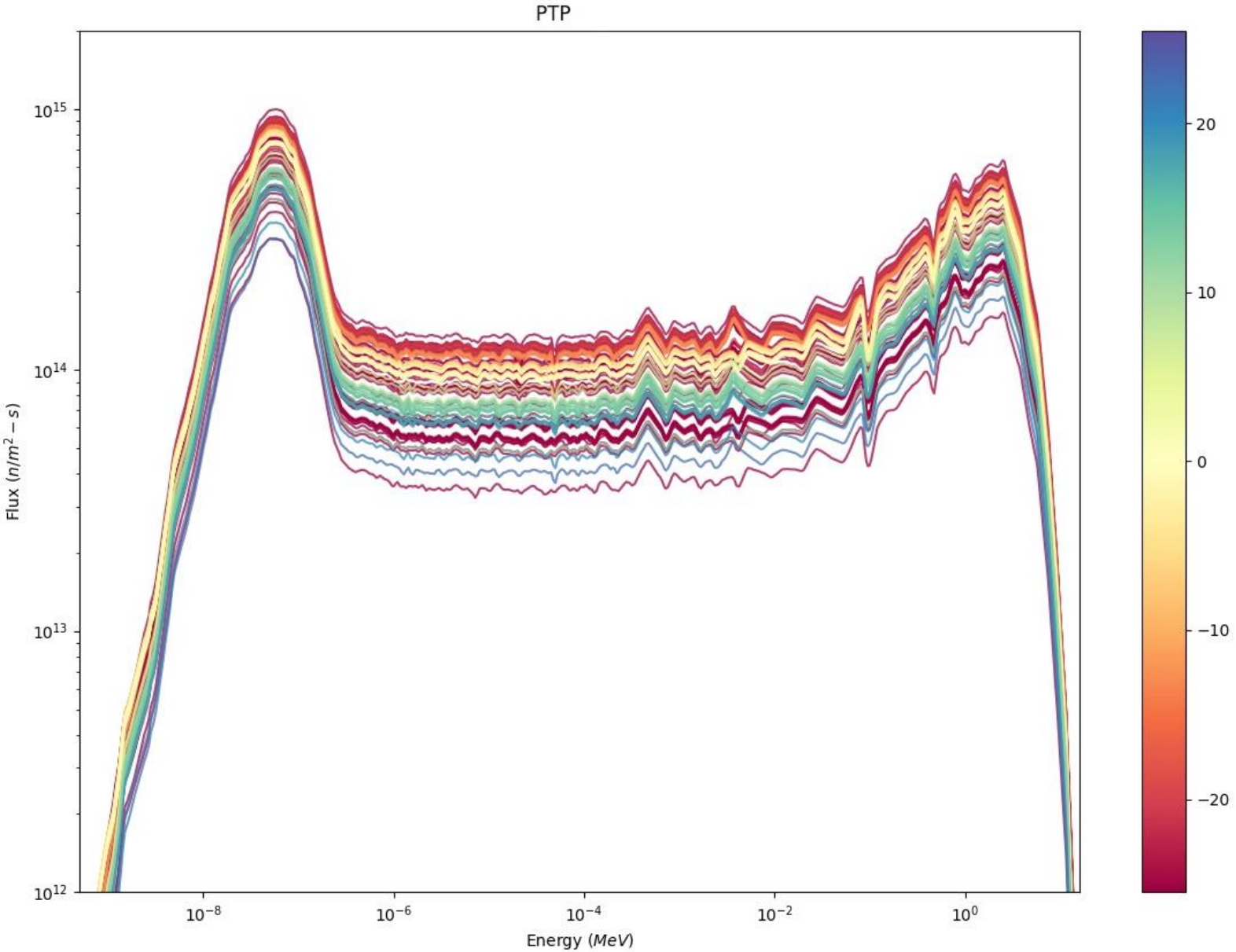


Figure 11: A combined flux profile of all of the samples located in the PTP Region

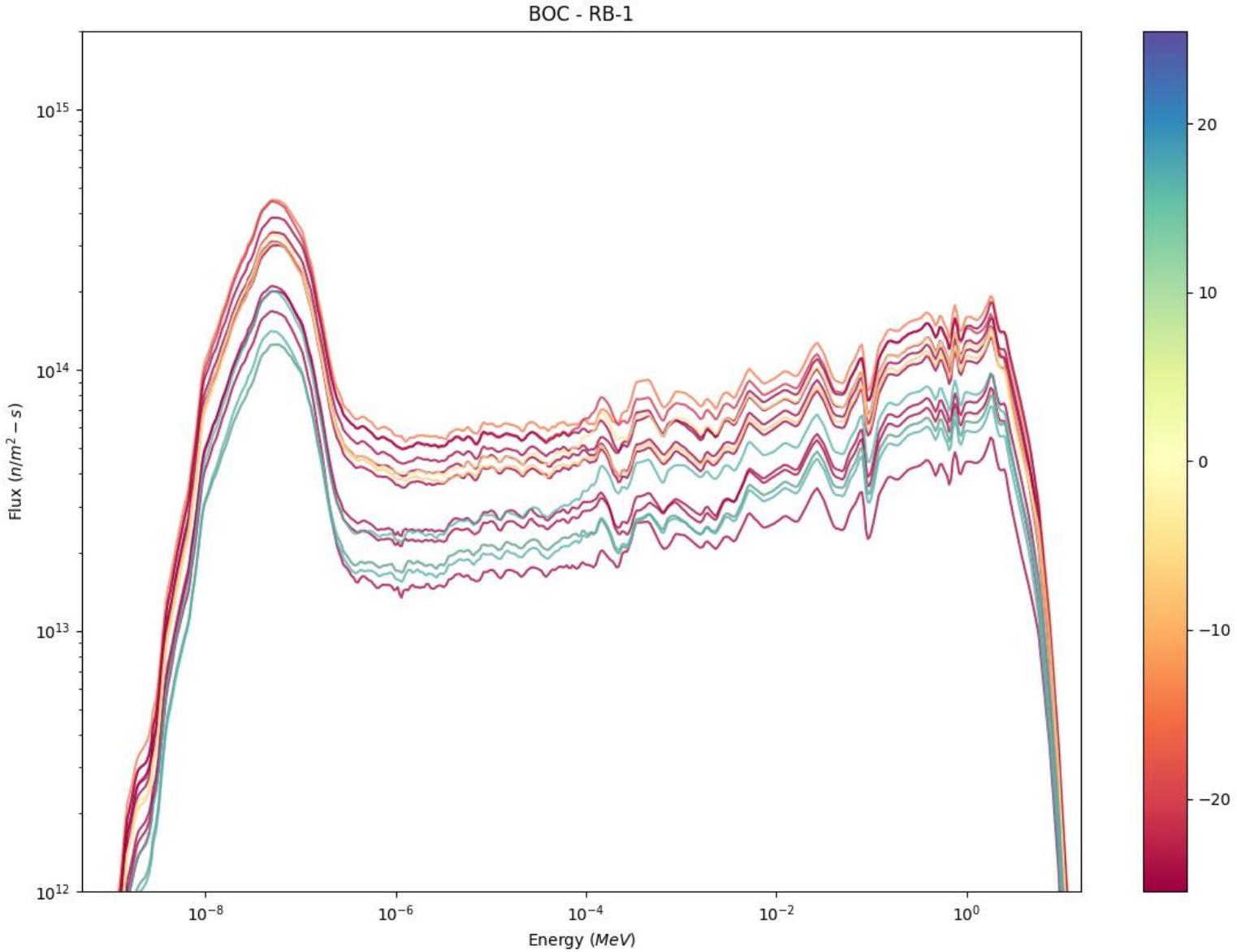


Figure 12: A combined flux profile of all of the samples located in the RB-1 Region for BOC

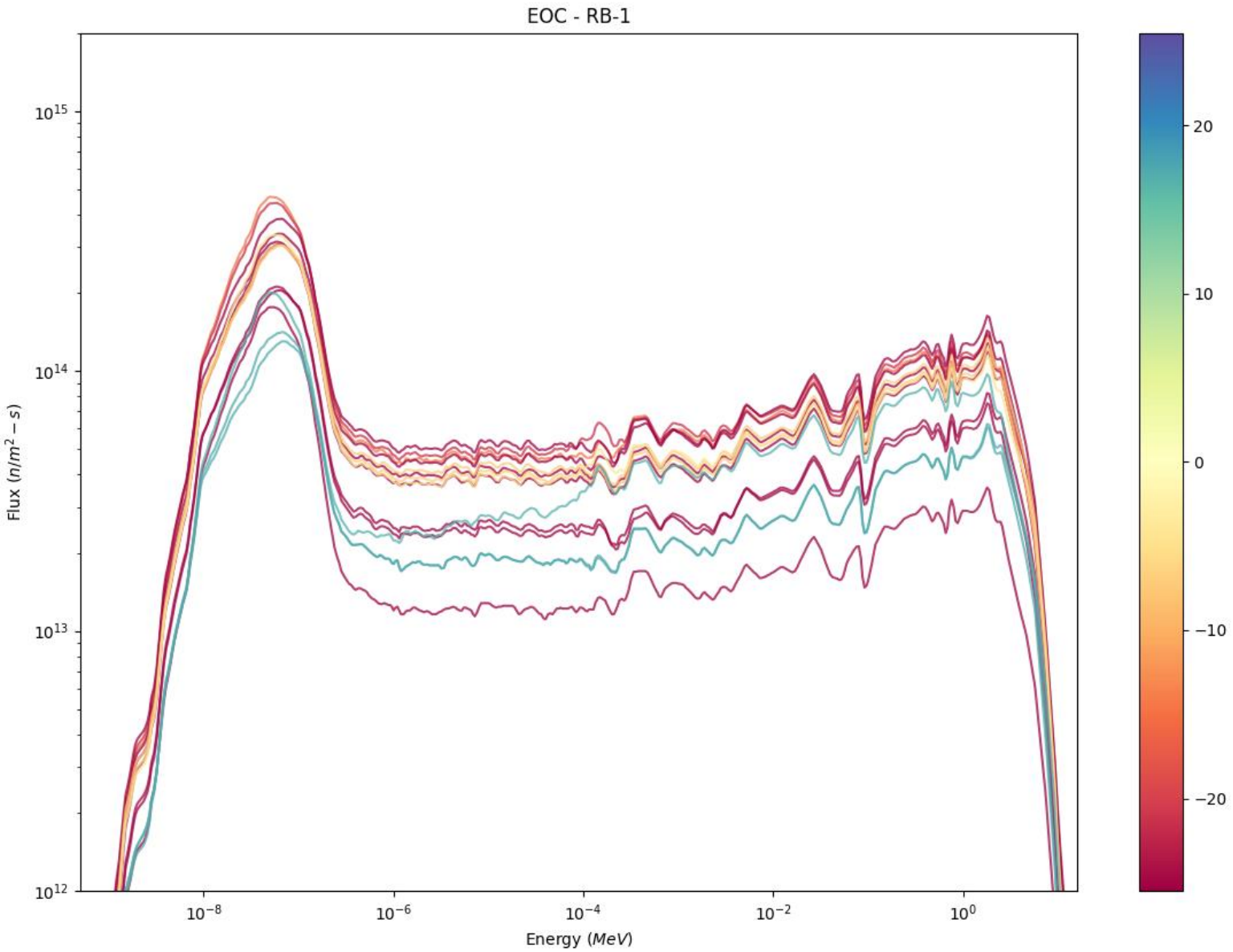


Figure 13: A combined flux profile of all of the samples located in the RB-1 Region for EOC

4.3 FT-5 Comparison

In order to get a clear picture of how axial distance from centerline affects the neutron flux profile, Section 4.3 shows the neutron flux for various sub-regions of the FT. This was also be able to show how variability differs between sub-regions. The FT was chosen because it was broken into symmetrical sub-regions around the centerline, and the sub-regions could be combined into absolute distance from centerline.

Figure 14 only has a few available samples as these are located the furthest from the centerline, but since they are all almost the same distance away this showcases how other uncertainties affect the neutron flux profile. The most important factor in the variance comes from the MW differences of the cores between the samples mentioned in Section 2.1, with the 85 MW samples having an overall lower flux on average. The magnitude of these samples is significantly lower than the samples close to centerline with thermal peaks closer to ~10^{15}. Very little variability is seen in the thermal region with the noticeable differences in the fast region. This shows that the samples were affected more by the differences in activation rate for the high energy reactions.

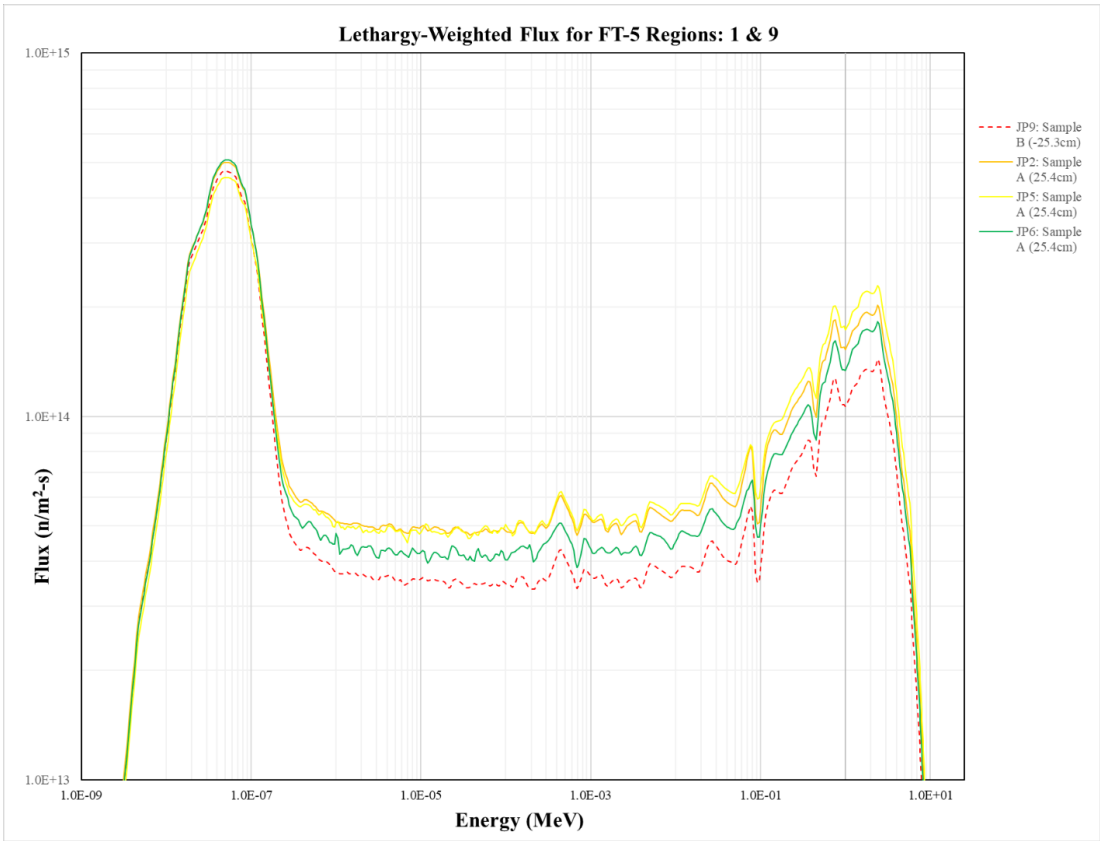


Figure 14: Flux profile for FT-5 samples > 23 cm from centerline

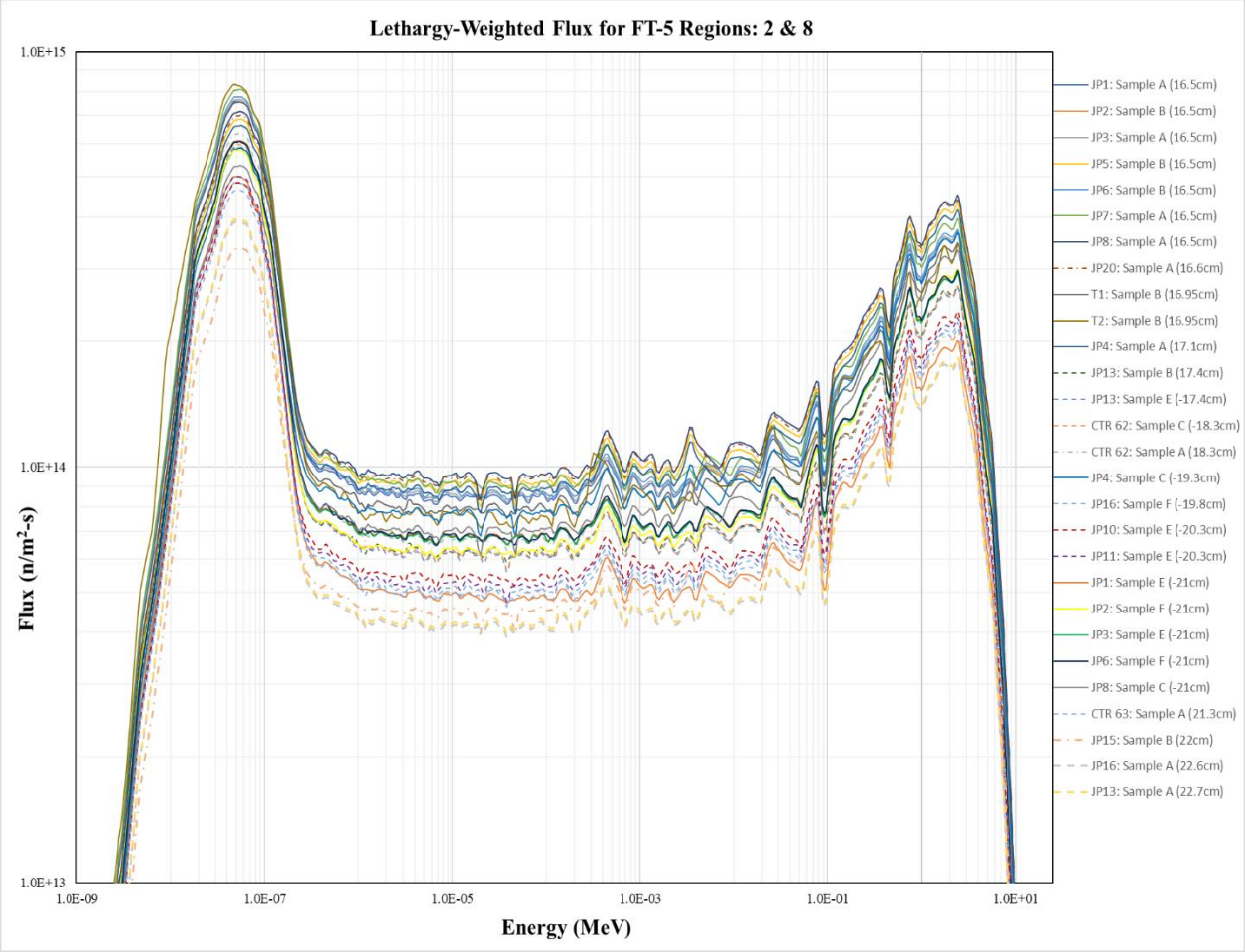


Figure 15: Flux profile for FT-5 samples between 16.5 & 22 cm from centerline

Figure 15, this is where a large portion of the samples are located. The magnitude of these samples has gone up considerably from the previous group but is still short of the overall peak (~10^{15}). There is an increase in variability in the thermal region along with similar or slightly less in the fast region. The difference in power levels and how it affects variance is more visible in this range. The range in this group is fairly large, so a portion of the increased variability is due to comparing samples up to 6 cm apart.

Figure 16 shows a slight increase in magnitude from the second group. The variability in the thermal and fast regions decreased as the range moved closer to the centerline. The small group of samples slightly above the main group of samples belongs to the corrected JP 1-8 experiments. All of the samples are at +/- 12.1 cm and should be located at the top of the grouping but are slightly higher than expected due to both the difference in power levels and uncertainties in the correction. Section 4.4 goes into more detail about the corrections made.

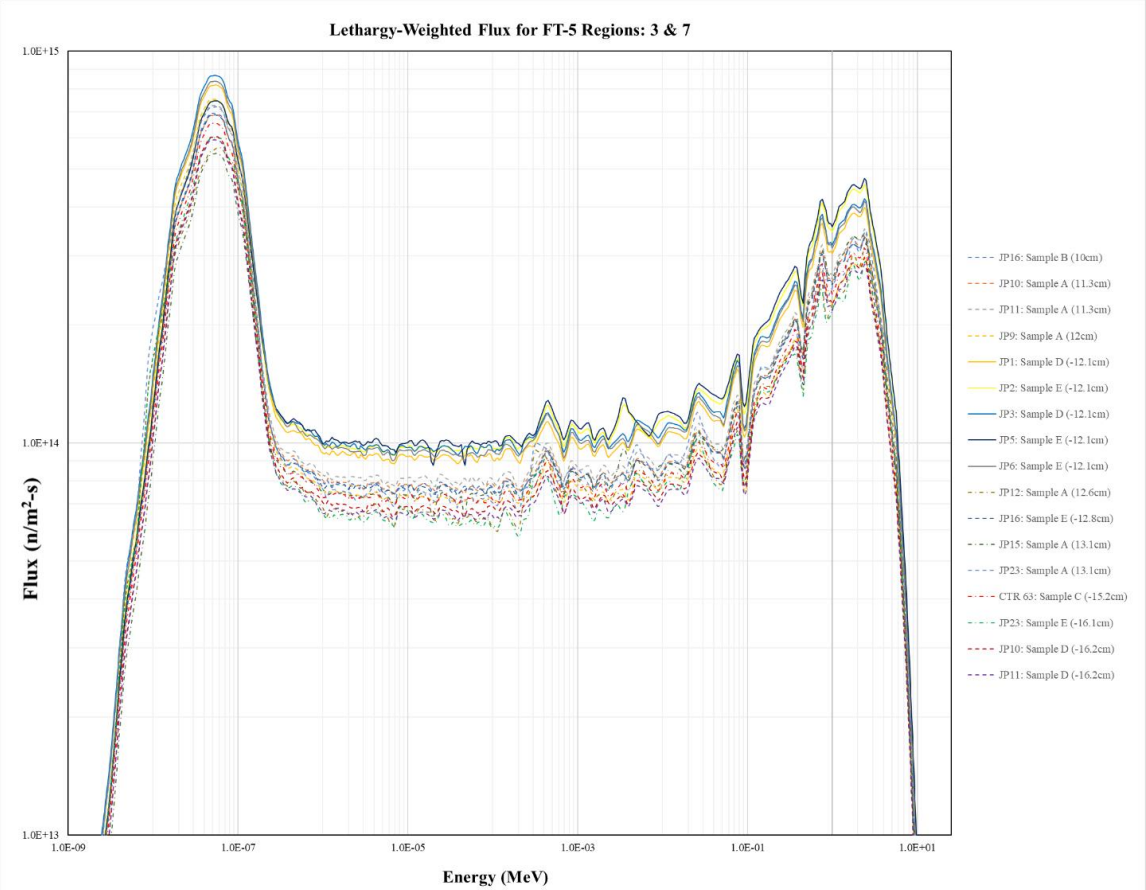


Figure 16: Flux profile for FT-5 samples between 10 & 16.5 cm from centerline

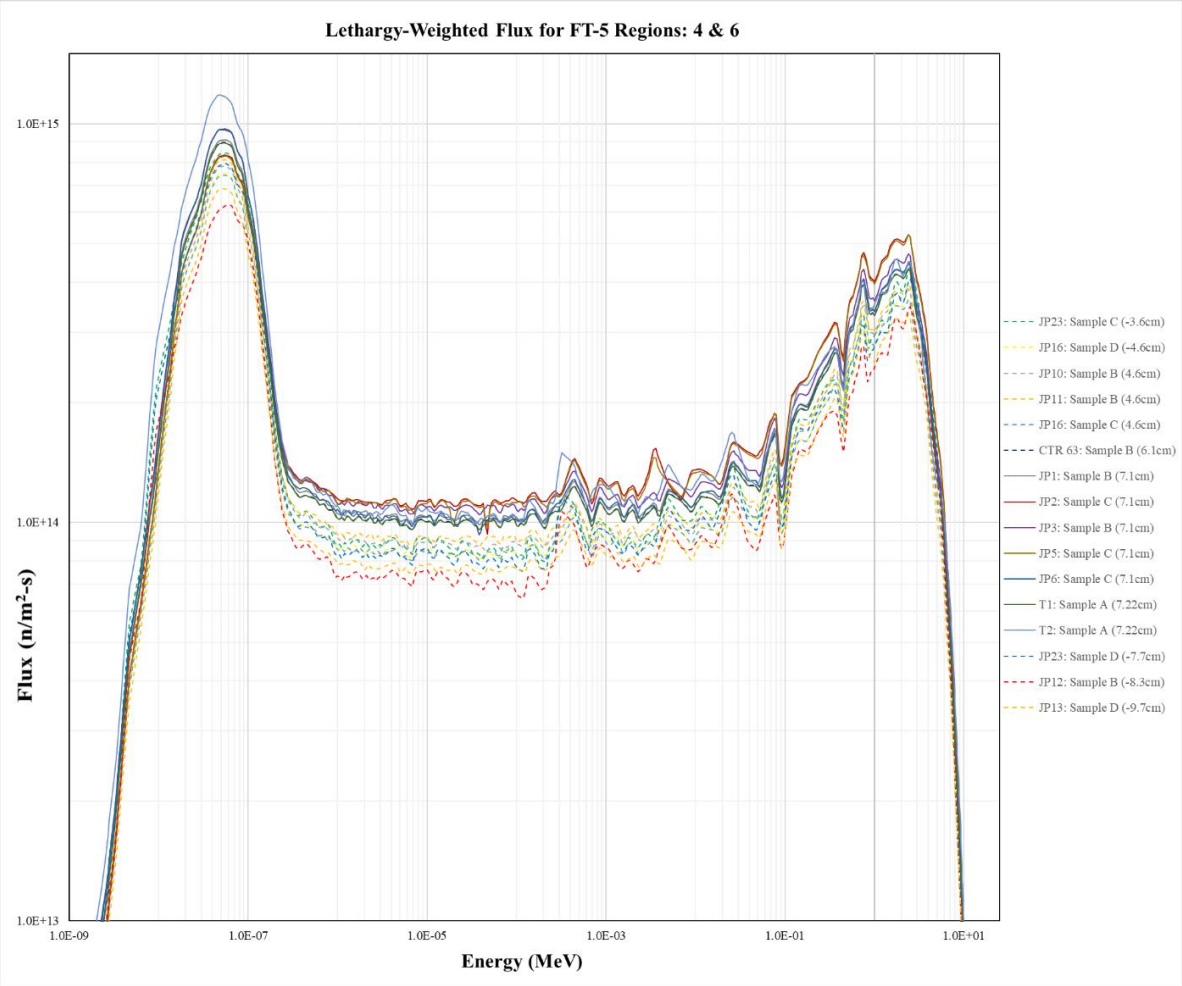


Figure 17: Flux profile for FT-5 samples between 3 & 10 cm from centerline

Figure 17 shows a slight increase in magnitude from the previous group. The variability in the thermal and fast regions continued to decrease as the range moved closer to the centerline. The difference in power levels is still visible in this range. The sample with the highest magnitude in the thermal region belongs to T2: Sample A. This is above the expected magnitude for its axial height more than likely because it does not contain a sample wire with a reaction in the thermal region. Because all of the activation reactions in the wire represent threshold reactions (with energies well above the thermal range), it cannot properly map the thermal region.

Figure 18 shows a slight increase in magnitude from the previous group reaching the peak for the FT region. The trend continues with a noticeable decrease in variability across the entire energy spectrum and a distinction between the samples from the 85 and 100 MW cores.

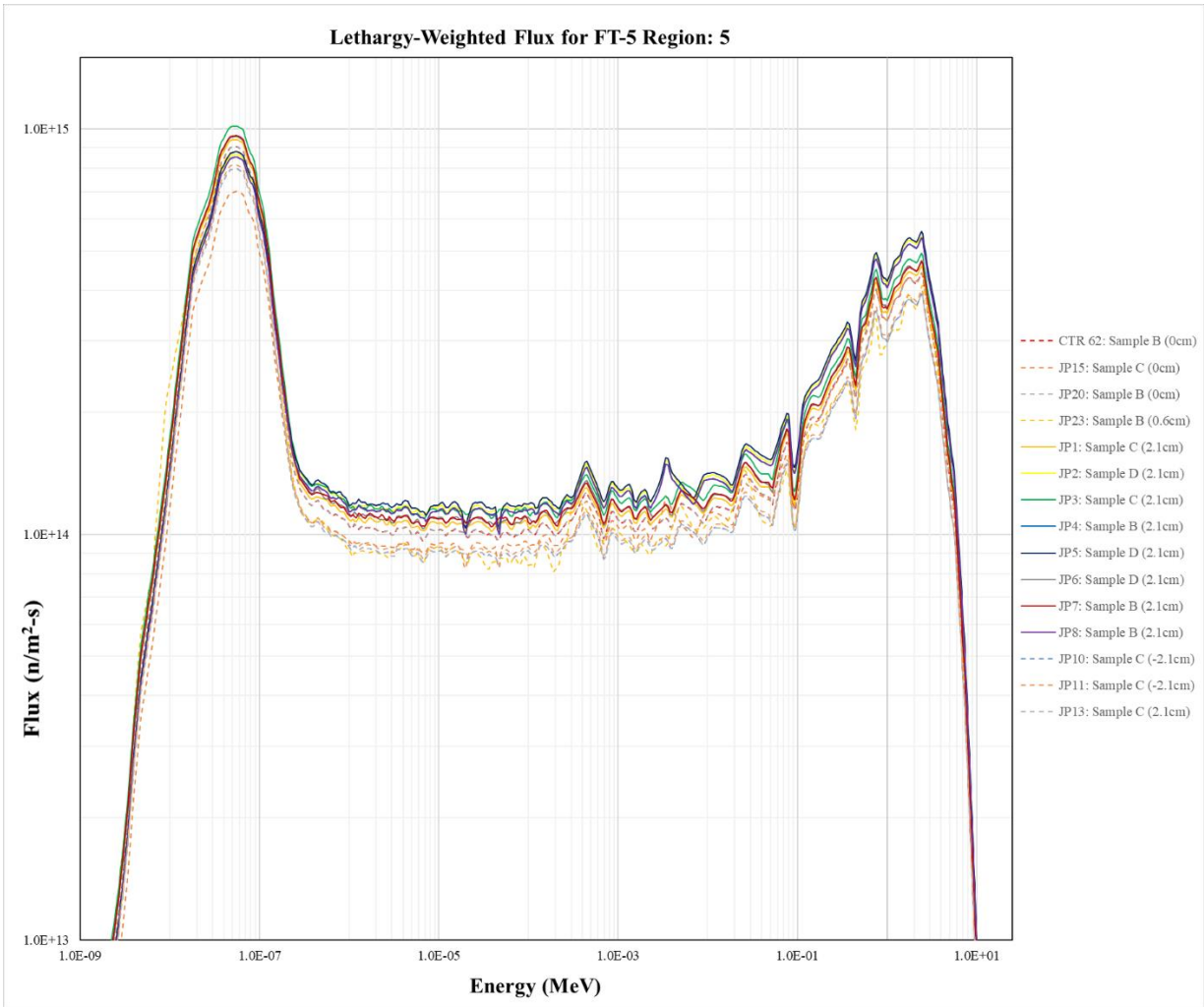


Figure 18: Flux profile for FT-5 samples < 3 cm from centerline

Overall, utilizing samples from more than 15 different experiments shows there is a noticeable trend in decreasing variability of the neutron flux as the samples gets closer to the centerline of the core. This holds true for the entire energy spectrum. There is also a clear distinction between samples from the 85 MW and the 100 MW cores, demarcating a difference in irradiation environment.

4.4 JP1-8

When analyzing the historical experiments, several of the JP experiments in the FT-5 region resulted in noticeably high chi-squared results (>200). These experiments had similar exposure rates to other cases with low chi-squared values, with no other apparent reason for the poor results. Utilizing the other experiments in this analysis for comparison, there shows significant evidence that the activation rates reported in these experiments were documented incorrectly. From inspection, only two reactions were

misreported in the experiments: the 55Mn(n,2n)54Mn reaction and the 54Fe(n,p)54Mn reaction (both located in the fast region). For this analysis, the reactions were then corrected to accurately reflect the activation rates seen in similar experiments. The corrections are not exact but allowed for more reliable results. These corrected rates can be seen in Table 10.

Figure 19 shows the neutron flux profiles for the original and corrected JP 1-8 experiments. The lines in blue are the original values, and the red lines are the corrected values. The dotted black line is the average neutron flux value for the FT-5 region. This clearly shows a significant difference between the corrected and original activation rates. Some of the samples saw changes of more than an order of magnitude. Overall, the significant decrease in chi-squared values, that are now comparable with other samples in the FT region, justify the changes in activation rates.

Table 14: JP 1-8 Updated activation results

Experiment	Reaction	Previous Activation Rate	New Activation Rate
JP1	55Mn(n,2n)54Mn	x 10^{-12}	x 10^{-13}
JP2	54Fe(n,p)54Mn	x 10^{-9}	x 10^{-11}
	55Mn(n,2n)54Mn	x 10^{-8}	x 10^{-13}
JP3	55Mn(n,2n)54Mn	x 10^{-12}	x 10^{-13}
JP4	55Mn(n,2n)54Mn	x 10^{-14}	x 10^{-13}
JP5	55Mn(n,2n)54Mn	x 10^{-14}	x 10^{-13}
JP6	54Fe(n,p)54Mn	x 10^{-9}	x 10^{-11}
	55Mn(n,2n)54Mn	x 10^{-8}	x 10^{-13}
JP7	54Fe(n,p)54Mn	x 10^{-9}	x 10^{-11}
	55Mn(n,2n)54Mn	x 10^{-8}	x 10^{-13}
JP8	55Mn(n,2n)54Mn	x 10^{-14}	x 10^{-13}

Table 15: JP 1-8 Original and corrected result comparison

Experiment	Sample ID	Height (cm)	Region Used	Original Chi-Squared	Corrected Chi-Squared
JP1	A	16.5	8	226.4	0.50
	B	7.1	6	244.1	3.97
	C	2.1	5	246.1	2.72
	D	-12.1	3	236.8	1.98
	E	-21	2	218.7	0.67
JP2	A	25.4	9	714.3	0.06
	B	16.5	8	713.8	1.02
	C	7.1	6	714.6	1.09
	D	2.1	5	716.0	1.73
	E	-12.1	3	715.7	1.27
	F	-21	2	714.0	0.50
JP3	A	16.5	8	229.4	0.72
	B	7.1	6	237.2	1.48
	C	2.1	5	229.7	1.10
	D	-12.1	3	223.9	0.59
	E	-21	2	224.3	1.33
JP4	A	17.1	8	718.8	3.41
	B	2.1	5	730.0	1.24
	C	-19.3	2	711.9	4.59
JP5	A	25.4	9	8.39	8.39
	B	16.5	8	755.1	2.52
	C	7.1	6	876.0	0.04
	D	2.1	5	772.6	0.92
	E	-12.1	3	750.3	1.24
JP6	A	25.4	9	713.8	1.13
	B	16.5	8	715.2	1.52
	C	7.1	6	715.6	6.46
	D	2.1	5	715.9	6.39
	E	-12.1	3	715.2	3.65
	F	-21	2	714.6	0.97
JP7	A	16.5	8	714.7	0.92
	B	2.1	5	716.5	5.40
JP8	A	16.5	8	783.4	2.88
	B	2.1	5	790.8	2.80
	C	-21	2	804.7	8.99

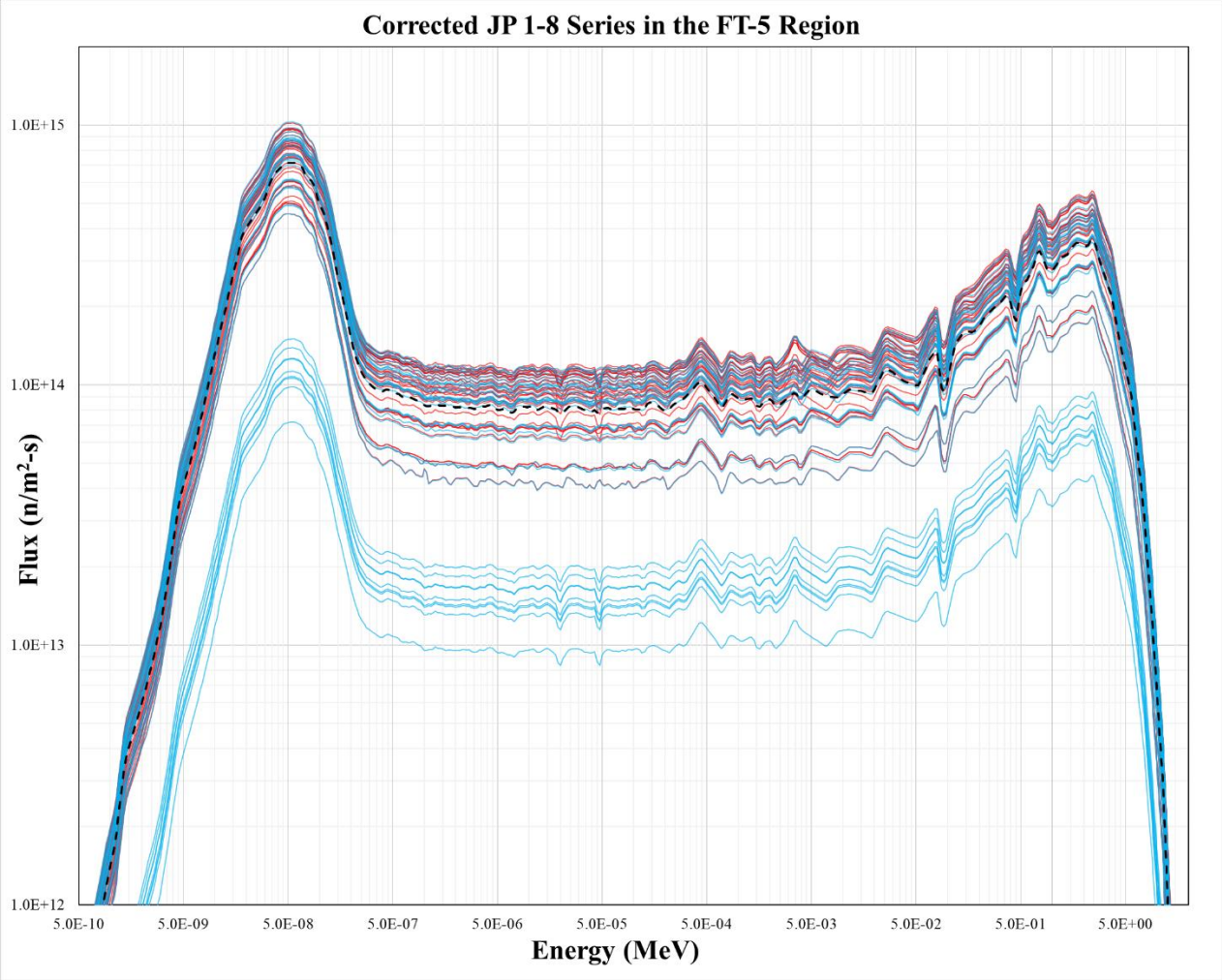


Figure 19: Flux profile for original (blue) and corrected (red) JP 1-8 experiments. Dotted black line – Average of the neutron flux in FT-5 region

4.5 Conclusion

The goal of this analysis was to categorize the HFIR neutron flux by comprehensively documenting the wealth of historical measurement data of HFIR experiments and creating an accurate and traceable summary of experimental information. In addition, the historical experiments were to be reanalyzed by utilizing updated ENDF nuclear data libraries, created specifically for this analysis, on these historical experiments in order to improve current models of the HFIR flux spectrum and increase precision for future experiments. An improved understanding of the neutron flux in HFIR will help identify gaps in uncertainty where current knowledge needs to improve and support a reliable method for analyzing how the samples interact with other material while in the

core. With proper understanding, the HFIR spectra could be used for production-quality measurements of fundamental nuclear data in the future.

A focal point was creating a methodology for experiment information indexing by categorizing the flux into different regions, sample wire materials (reactions), and axial locations to help create a detailed summary of important information of the experiments that take place in HFIR and allowing for more accurate comparison over time.

This was accomplished by reviewing the historical experiments and extracting the relevant information. For this analysis it was the: dates, exposure, sample material, experiment location, and activation rates. This allowed for the samples to be broken up into relevant categories for analyzation. Next, the updated ENDF libraries for STAYSL PNNL were compiled using the most current nuclear data for the relevant reactions. The libraries were formatted in a STAYSL friendly standard 725-group library that would provide a neutron flux spectrum that gives the best fit for the measured activities maximizing granularity. On top of the 725-group library, a second user-specified 252-group grid was specified as the desired output from STAYSL PNNL, because it is the industry standard for the Light Water Reactor (LWR) spectrum.

This MCNP model based on HFIR mentioned in Section 3.7.2, was used to create an initial guess spectrum for each sample. All of the regions follow a similar shape with the distinct difference being the increased flux magnitudes at locations closer to center of the flux trap region. Each sample was then run through STAYSL PNNL to create a neutron flux profile and provide a chi-squared value. They were then documented to allow for proper analysis and comparison.

This analysis also aimed to study how the neutron flux spectrum varied with location, both spatially and radially, as well as investigating biases in prior flux shape estimates arising from older nuclear data evaluations. There are several key trends seen in the analysis:

- The FT-5 Region follows the expected flux shape from the initial guess spectrum and shows low levels of variability in neutron flux across each sub-region.
- The PTP region also followed the expected flux shape from the initial guess spectrum. Again, there are differences in magnitude between the axial sub-regions, however, compared to the FT region you can see less variability between the samples with each sub-region tightly grouped together. Overall, the PTP Region also shows low levels of variability in neutron flux.
- The RB-1 region also followed the expected shape from the initial guess spectrum. From inspection, there is virtually no difference between the BOC and EOC samples besides minor magnitude differences. In contrast to the FT and PTP regions, there is a noticeable difference in neutron flux magnitude in relation to the axial distance from centerline. This is evident looking at how the samples separated into two groups with the bottom group consisting of samples located more than 15 cm from the centerline. This trend continues for entire energy

spectrum but is more noticeable in the thermal and epi-thermal regions. Even with these differences, the RB-1 region also shows a low overall level variability in neutron flux, with the condition of being more sensitive to axial differences than the FT-5 and PTP regions.

- Overall, there is a noticeable trend in variability decreasing for the neutron flux as the samples gets vertically closer to the centerline of the core. This holds true for each region across the entire energy spectrum.
- Section 4.3 shows that there is also a clear delineation between samples from the 85 MW and the 100 MW cores. This implies they have distinct irradiation environments. Not only is this important for cataloging samples and use in future analysis, but it would imply that the variance in the spectrum shape is actually smaller than what figures in Section 4.2 would have you believe and that the spectrum shape has been changed. It should be noted that this is really only applies for the FT-5 since the PTP and RB regions do not have a significant amount of sample data from the 85 MW core.
- The results show magnitude differences in the neutron flux between the different radial regions, with it decreasing as you move away from the center of the core. However, there is no noticeable variance in shape between the different regions.
- For each region, the chi-squared values for the fitted flux shapes remain low. Outside of a few outliers, the average reduced chi-squared value is below five. This would imply that STAYSL was able to find a neutron spectrum that fit well for each sample across all three major regions.
- In addition to data analyzed in the different region, it was discovered that significant evidence points to activation rates reported in the JP 1-8 experiments were documented incorrectly. With the correction performed in Section 4.4, there was a notable decrease in chi-squared values, with them now being comparable to the other samples in the FT region. This evidence leads to justifying the changes in activation rates made in this analysis.
- Compared to all of the other reactions, the Mn55(n,2n)Mn54 reaction had the highest level of uncertainty in activation rates. The most likely explanation for this is the level of reliability of data for high-energy reactions compared to the more well-defined thermal region.

Future work would include additional reanalysis of historical experiments, and de-convoluting the axial factor correction to allow for further investigation. In particular, it would be beneficial to include cases with exact location information and samples reactions that have yet to be documented. Now that the data is categorized into a single location re-analysis will be much simpler. New experiments in HFIR could be aimed directly at addressing gaps in the HFIR spectra knowledge. The goal would be to expand to include new information and deepen the current understanding. With enough information, the HFIR spectra could be used for production-quality measurements of fundamental nuclear data.

LIST OF REFERENCES

1 Batchelder, J., Kawano, T., Kelley, J., Kondev, F. G., McCutchan, E., Smith, M., Sonzogni, A., Thoennessen, M., and Thompson, I. White Paper on Nuclear Data Needs and Capabilities for Basic Science. United States: N. p., 2017. Web. doi:10.2172/1358313.

2 ORNL, High Flux Isotope Reactor (HFIR) User Guide Rev 2.0 (2015)

3 Mahmood, S T, Mirzadeh, S, Farrell, K, Pace, III, J V, and Oliver, B M, Neutron dosimetry of the HFIR hydraulic facility. United States: N. p., 1995. Web. doi:10.2172/34421.

4 Garland, M.A. & Mirzadeh, Saed & Alexander, C.W. & Hirtz, G.J. & Hobbs, R.W. & Pertmer, G.A. & Knapp, F.F.. (2003). Neutron flux characterization of a peripheral target position in the High Flux Isotope Reactor. Applied radiation and isotopes : including data, instrumentation and methods for use in agriculture, industry and medicine. 59. 63-72. 10.1016/S0969-8043(03)00144-1.

5 Mirzadeh, S, Callahan, A P, Knapp, Jr, F F, and Schenter, R E, Production capabilities in US nuclear reactors for medical radioisotopes. United States: N. p., 1992. Web. doi:10.2172/10191510.

6 Greenwood, Lawrence R, and Johnson, Christian D. User Guide for the STAYSL PNNL Suite of Software Tools. United States: N. p., 2013. Web. doi:10.2172/1067961.

7 L. R. Greenwood, Neutron Source Characterization for Materials Experiments, Alloy Development for Irradiation Performance, DOE/ER-0045/11, pp. 30-37 (1983).

8 L. R. Greenwood, Neutron Source Characterization for Materials Experiments, Alloy Development for Irradiation Performance, DOE/ER-0045/13, pp. 13-17 (1984).

9 L. R. Greenwood, Neutron Dosimetry and Damage Calculations, Alloy Development for Irradiation Performance, DOE/ER-0045/16, pp. 17-24 (1986).

10 L. R. Greenwood, Fission Reactor Dosimetry – HFIR – CTR31, 32, 34, and 35, Damage analysis and fundamental studies. Vol. 1. Quarterly progress report, DOE/ER-0046/13, pp. 17-26 (1983).

11 L. R. Greenwood, Fission Reactor Dosimetry – HFIR – CTR 40-45, Damage analysis and fundamental studies. Vol. 1. Quarterly progress report, DOE/ER-0046/19, pp. 5-8 (1984).

12 L. R. Greenwood, Fission Reactor Dosimetry - HFIR - CTR 30, 36, 46, Damage analysis and fundamental studies. Vol. 1. Quarterly progress report, DOE/ER-0046/21, pp. 5-9 (1985).

13 L. R. Greenwood, Dosimetry and Damage Analysis for HFIR-CTR-47/48, Fusion Reactor Materials Semiannual Progress Report, DOE/ER-0313/2, pp. 38-40 (1987).

14 L. R. Greenwood, Measurements for the JP2, JP6, JP7 US/Japanese Experiments in HFIR, Fusion Reactor Materials Semiannual Progress Report, DOE/ER-0313/2, pp. 31-33 (1987).

15 L. R. Greenwood and C. A. Seils, Dosimetry and Damage Calculations for the JP4, JP5, and JP8 US/Japanese Experiments in HFIR, Fusion Reactor Materials Semiannual Progress Report, DOE/ER-0313/3, pp. 30-32 (1987).

16 L. R. Greenwood and D. V. Steidl, Dosimetry for The HFIR - CTR 53/54 Experiments, Fusion Reactor Materials Semiannual Progress Report, DOE/ER-0313/8, pp. 40-42 (1990).

17 L. R. Greenwood and R. T. Ratner, Neutron Dosimetry and Damage Calculations for the JP-10, 11, 13, and 16 Experiments in HFIR, Fusion Reactor Materials Semiannual Progress Report, DOE/ER-0313/19, pp. 281-285 (1995).

18 L. R. Greenwood and R. T. Ratner, Neutron Dosimetry and Damage Calculations for the JP-17, 18, and 19 Experiments in HFIR, Fusion Reactor Materials Semiannual Progress Report, DOE/ER-0313/19, pp. 286-290 (1995).

19 L. R. Greenwood and R. T. Ratner, Neutron dosimetry and damage calculations for the HFIR-JP-23 irradiations, Fusion Reactor Materials Semiannual Progress Report, DOE/ER-0313/21, pp. 229-232 (1996).

20 L. R. Greenwood and C. A. Baldwin, Neutron Dosimetry and Damage Calculations for the HFIR-JP-9, -12, and -15 Irradiations, Fusion Reactor Materials Semiannual Progress Report, DOE/ER-0313/23, pp. 301-304 (1997).

21 L. R. Greenwood and C. A. Baldwin, Neutron Dosimetry and Damage Calculations for the HFIR-JP-20 Irradiation, Fusion Reactor Materials Semiannual Progress Report, DOE/ER-0313/23, pp. 305-308 (1997).

22 L. R. Greenwood and C. A. Baldwin, Neutron Dosimetry and Damage Calculations for the HFIR-CTR-62 and 63 Irradiations, Fusion Reactor Materials Semiannual Progress Report, DOE/ER-0313/26, pp. 199-201 (1999).

23 L. R. Greenwood and C. A. Baldwin, Neutron Dosimetry and Damage Calculations for the TRIST ER-1 Experiment in HFIR, Fusion Reactor Materials Semiannual Progress Report, DOE/ER-0313/26, pp. 194-198 (1999).

24 Xoubi, Ned & Primm, Trent. (2005). Modeling of the High Flux Isotope Reactor Cycle 400.

VITA

Austin Stanford grew up in the small town of Soddy Daisy, Tennessee, where his interest in science started at a very young age. When it was time to think about possible college majors, he was heavily influenced by his close proximity to the Sequoyah Nuclear Power Plant. After learning more about nuclear energy and its contribution to carbon-free energy generation, he decided to attend the University of Tennessee, Knoxville (UTK) because of its highly regarded nuclear engineering program. During his time at UTK, Austin worked on several different nuclear research projects, but ultimately decided to pursue a master's degree with a focus on nuclear reactor analysis and nuclear security under the supervision of Dr. Steven Skutnik. During his first year, he began work on a project in collaboration with HFIR, which quickly became the work of his thesis. Austin now lives in Chicago with his wife and dog, working for an engineering company focused on supporting nuclear plants and facilities.